

STATISTICAL DESCRIPTION OF SYNCHROTRON INTENSITY FLUCTUATIONS: STUDIES OF ASTROPHYSICAL MAGNETIC TURBULENCE

A. LAZARIAN

Department of Astronomy, University of Wisconsin, Madison, US

D. POGOSYAN

Physics Department, University of Alberta, Edmonton, Canada

Draft version October 28, 2018

ABSTRACT

We provide a theoretical description of synchrotron fluctuations arising from magnetic turbulence. We derive an expression that relates the correlation of synchrotron fluctuations for an arbitrary index of relativistic electrons to the correlations arising from a particular $\gamma = 2$ index that provides synchrotron emissivity proportional to the squared intensity of perpendicular to the line of sight component of magnetic field. We provide a detailed study of the statistics in the latter case assuming that the underlying magnetic turbulence is axisymmetric. We obtain general relations valid for an arbitrary model of magnetic axisymmetric turbulence and analyze the relations for the particular example of magnetic turbulence that is supported by numerical simulations. We predict that the synchrotron intensity fluctuations are anisotropic with larger correlation present along the direction of magnetic field. This anisotropy is dominated by the quadrupole component with the ratio between quadrupole and monopole parts being sensitive to the compressibility of underlying turbulence. Our work opens avenues for quantitative studies of magnetic turbulence in our galaxy and beyond using synchrotron emission. It also outlines the directions of how synchrotron foreground emission can be separated from cosmological signal, i.e. from CMB or highly redshifted HI emission. For the sake of completeness we also provide the expressions for the synchrotron polarization (Stocks parameters and their combinations) for the model of axisymmetric magnetic turbulence.

Subject headings: turbulence – ISM: general, structure – MHD – radio continuum: ISM.

1. INTRODUCTION

Synchrotron fluctuations both carry information about magnetic fields and interfere with the measurements of cosmic microwave emission (CMB) as well as with attempts to measure enigmatic emission from atomic hydrogen (HI) in the early Universe. Therefore it is essential to have proper description of the statistics of synchrotron fluctuations. This paper concentrates on the statistical properties of the synchrotron intensities arising from turbulent magnetic fields.

Galactic and extragalactic synchrotron emission arises from the interaction of astrophysical magnetic fields and cosmic rays (see Ginzburg 1981). In terms of CMB and high redshift HI studies, the most important are galactic synchrotron emission. This emission provides the largest range of scales for studying magnetic fields. Magnetic fields are turbulent as observations testify that turbulence is ubiquitous in astrophysics (Armstrong et al. 1995; Lazarian 2009; Chepurnov & Lazarian 2010). As relativistic electrons are present in most cases, the turbulence results in synchrotron fluctuations, which may provide detailed information about magnetic fields at different scales, but, at the same time, impede measures of CMB and high redshift HI. The latter has become a direction of intensive discussion recently (see Loeb & Zaldarriaga 2004; Pen et al. 2008; Loeb & Wyithe 2008; Liu et al. 2009).

Present and future big telescopes, e.g. Square Kilometer Array (SKA), LOw Frequency ARray (LOFAR), are designed to map synchrotron emission with unprecedented resolution and sensitivity. Therefore it is absolutely crucial that the information available with these instruments is being used to get better insight fundamental astrophysical processes.

Properties of turbulent magnetic fields that influences most of the processes in diffuse astrophysical environments are very much desired through the corresponding studies. The obstacle for such studies is that the relation between the underlying turbulence and the synchrotron fluctuations is not trivial because the synchrotron intensity depends both on magnetic field H and on the power index α of relativistic electrons, which emit radiation spiraling in magnetic field. The physics of emission is rather non-trivial which results in the expression of synchrotron intensity which are proportional to magnetic field in a fractional power, H^γ , $\gamma = 1/2(\alpha + 1)$ that has been an impediment for a correct description of synchrotron fluctuations.

For instance, studies of synchrotron intensity fluctuations in the Milky Way (see Cho & Lazarian 2010 and references therein) reveal power law spectra that can be related to magnetic turbulence. How are these spectra related to the underlying spectra of magnetic fluctuations? What is the effect of the electron spectral index on the result? Are the fluctuations of magnetic field related to compressions or have Alfvénic nature? Are there additional information apart from the magnetic spectrum one can obtain from synchrotron fluctuations? These are the questions that we are going to address in the paper.

A number of attempts to describe synchrotron fluctuations has been attempted assuming that $\gamma = 2$, which provides an approximation to the actual index of galactic synchrotron emission (see Getmantsev 1959; Chibisov & Ptuskin 1981; Lazarian & Shutenkov 1990; Lazarian & Chibisov 1991; Chepurnov 1998). Some of these papers (e.g. Getmantsev 1959; Chepurnov 1998) did not consider mean magnetic field while others dealt with the spectrum of fluctuations that arise from unrealistic idealized isotropic magnetic turbulence. As we discuss further, such an isotropic model contradicts the current understanding of magnetic turbulence.

An attempt to take anisotropy into account was made in Lazarian & Shutenkov (1990), where the anisotropy of the synchrotron fluctuations was analyzed and the quadruple component of the spatial decomposition of the synchrotron correlations was used to study the spectrum of synchrotron fluctuations. The work used the explicit integral equations solving the inverse problem for the magnetic fluctuations, but the anisotropy was introduced in the problem by assuming that the magnetic field can be presented as a superposition of a regular and isotropic random magnetic fields. The latter assumption was not supported by the later numerical and theoretical research.

In short, the limitations of all earlier studies were related both to the incorrect models of astrophysical turbulence and to the constraints arising from doing calculation just for a single cosmic ray electron index $\gamma = 2$. The magnetic turbulence is known to be anisotropic and the actual index may substantially differ from that single chosen value and it is not clear how accurate the description of synchrotron fluctuations stays for γ not equal to 2.

The goal of this paper is to address both of the deficiencies of the earlier studies. First of all, recent years have been marked by important advances in the theory of compressible MHD turbulence and its statistical description (e.g. Goldreich & Sridhar 1995; Lazarian & Vishniac 1999; Cho & Vishniac 2000; Maron & Goldreich 2001; Lithwick & Goldreich 2001; Cho et al. 2002; Cho & Lazarian 2002, 2003; Kowal & Lazarian 2010). This understanding of turbulence should be included in the description of synchrotron fluctuations. In addition, it is absolutely vital to understand what is happening with the synchrotron statistics for γ different from the single value of $\gamma = 2$ that was the focus of the earlier studies.

Our paper relates synchrotron fluctuations with realistic magnetic turbulence for arbitrary electron power law index extending the reliability of magnetic field studies. We also propose new ways of studying magnetic fields, in particular, separating contributions from compressible and incompressible magnetic fluctuations.

In this paper we do not directly address the synchrotron polarization studies. We, however, should mention that the existing studies attempting to answer important questions about magnetic fields, e.g. question of magnetic helicity, using synchrotron (see Waelkens, Schekochihin & Enßlin 2009, Junklewitz & Enßlin 2011) suffer from the same limitations as the earlier statistical studies of synchrotron intensity, i.e. they also assume $\gamma = 2$ and isotropy of magnetic turbulence. We believe that our approach should be useful for these studies. To illustrate our point we address the problem of Faraday rotation measure fluctuations arising from anisotropic turbulence.

Our present paper is complementary to our work on probing turbulence using spectral measurements. In terms of those studies focused on recovering the spectrum of velocity turbulence from Doppler broadened absorption and emission lines (Lazarian & Pogosyan 2000, 2004, 2006, 2008) the present paper is intended to provide additional information about magnetic field fluctuations. This study is intended to provide the basis for the future development of techniques that recover turbulent statistics from observations using not only intensity, but other Stocks parameters of synchrotron emission.

Our study is intended to provide foundations for studying magnetic turbulence in the halo of Milky Way, in supernova remnants, in external galaxies as well as in clusters of galaxies (see Enßlin et al. 2010, 2009, Enßlin & Vogt 2006). As the resolution of telescopes gets higher detailed studies of turbulence in astrophysical jets, synchrotron emitting lobes get possible.

In §2 we justify the model of magnetic turbulence that we adopt, in §3 we describe the fluctuations of synchrotron emissivity and obtain general expressions for synchrotron fluctuations for an arbitrary spectral index of relativistic electrons. In §4 we analyse the anisotropy of synchrotron fluctuations arising from an arbitrary model of axisymmetric turbulence, while in §5 we show how this general treatment gets modified when a model of MHD turbulence that follows from numerical simulations is used. We discuss our results in §6 and provide our summary in §7. Appendixes are important part of these work. Apart from containing derivations related to the synchrotron intensity correlations they also contain the statistics of correlations of other Stocks parameters and useful combinations of the Stocks parameters (see Appendix E).

2. STATISTICAL DESCRIPTION OF MHD TURBULENCE: PERSPECTIVE OF AN OBSERVER

MHD Turbulence plays a crucial role for the processes of cosmic ray propagation (see Schlickeiser 2002; Longair 2011), star formation (see Elmegreen & Scalo 2004; McKee & Ostriker 2007), heat transfer in magnetized plasmas (see Narayan & Medvedev 2001; Lazarian 2006), magnetic reconnection (see Lazarian & Vishniac 1999; Kowal et al. 2009). Statistical description allows to reveal regular features within chaotic picture of turbulent fluctuations. The famous Kolmogorov description of incompressible hydrodynamic turbulence provides a vivid example of how turbulence complexity can be reduced to a simple formula $E(k) \sim k^{5/3}$, where $E(k)$ is an energy spectrum of turbulent motions.

MHD turbulence is more complex than the hydrodynamical one. Magnetic field defines the chosen direction of anisotropy (Montgomery & Turner 1981; Shebalin et al. 1983; Higdon 1984). For small scale motions this is true even in the absence of the mean magnetic field in the system. In this situation the magnetic field of large eddies defines the direction of anisotropy for smaller eddies. This observation brings us to the notion of *local system of reference*, which is one of the major pillars of the modern theory of MHD turbulence. Therefore a correct formulation of the theory requires wavelet description (see Kowal & Lazarian 2010). Indeed, a customary description of anisotropic turbulence

using parallel and perpendicular wavenumbers assumes that the direction is fixed in space. In this situation, however, the turbulence loses its universality in the sense that, for instance, the critical balance condition of the widely accepted model incompressible MHD turbulence (Goldreich & Sridhar 1995, henceforth GS95) which expresses the equality of the time of wave transfer along the magnetic field lines and the eddy turnover time is not satisfied¹.

MHD turbulence is a developing field with its ongoing debates². However, we feel that among all the existing models the GS95 provides the best correspondence to the existing numerical and observational data (see Beresnyak & Lazarian 2010; Chepurnov & Lazarian 2010). A limitation of the original GS95 model is that it assumes that the injection of energy happens with V_L equal to the Alfvén velocity V_A . In astrophysical situations turbulence can be injected with both $V_L < V_A$ and $V_L > V_A$. For the first case the turbulence starts initially in the regime of weak turbulence when Alfvénic perturbations weakly interact with each other. As scales of motions decrease, the strength of interactions, paradoxically, increases and the turbulence gets stronger. This regime was described analytically in Lazarian & Vishniac (1999, henceforth LV99). The regime $V_L > V_A$ is the regime of super-Alfvénic turbulence, when turbulence initially follows the Kolmogorov cascade and magnetic fields are not dynamically important. At smaller scales the turbulence gets into the strong MHD turbulence regime (see Lazarian 2006). We should add that the exact form of the magnetic correlation tensor does not follow from the GS95 model and should be obtained from numerical experiments. This was done in Cho et al. (2002) and Cho & Lazarian (2003).

The local system of reference is not accessible to an observer who deals with projection of magnetic fields from the volume to the pictorial plane. The projection effects inevitably mask the actual direction of magnetic field within individual eddies along the line of sight. As a result, the scale dependent anisotropy predicted in the GS95, which taking into our considerations above (see footnote 1) should be written as $\lambda_{\parallel} \sim L^{1/3} \lambda_{\perp}^{2/3}$, where λ_{\parallel} and λ_{\perp} are the parallel and perpendicular scale of the eddy, respectively, is not valid for the observer measuring parallel and perpendicular scales of projected and averaged along the line of sight eddies. As the observer maps the projected magnetic field in the global reference, e.g. system of reference of the mean field, the anisotropy of eddies becomes *scale-independent* and the degree of anisotropy gets determined by the anisotropy of the largest eddies which projections are mapped. This property of eddies being scale independent in the global system of reference is discussed in the earlier works (e.g. Cho et al. 2002; Esquivel & Lazarian 2005).

The testing of how ideas of incompressible MHD turbulence are applicable in the presence of compressibility was performed in Cho & Lazarian (2002, 2003) (also see Cho & Lazarian 2005, for a review). There, a decomposition of motions into basic MHD modes (Alfvénic, slow and fast) was performed to show that Alfvénic and slow modes keep the scaling of the incompressible MHD, while fast modes exhibit isotropy (see GS95, Lithwick & Goldreich 2001).

In a number of situations magnetic turbulence becomes isotropic for the observer. One of them is when the turbulence is super-Alfvénic, i.e. the velocity at the injection scale V_L is larger than the Alfvén speed V_A . Even in the opposite case, $V_A > V_L$, the observer may still detect isotropic turbulence if the line of sight is directed along the mean field in the volume. Super-Alfvénic turbulence may take place for molecular clouds (see Padoan et al. 2004) and clusters of galaxies (Brunetti & Lazarian 2007(@)).

In the presence of the mean magnetic field in the volume under study, an observer will see anisotropic turbulence, where statistical properties of magnetic field differ in the directions orthogonal and parallel to the mean magnetic field. The description of axisymmetric turbulence was given by Batchelor (1946), Chandrasekhar (1950) and later Matthaeus & Smith (1981) and Oughton et al. (1997). In our case it is natural to identify the axis of symmetry with the mean magnetic field and then the index-symmetric part of the correlation tensor can be presented in the following form:

$$\langle H_i(\mathbf{x}_1) H_j(\mathbf{x}_2) \rangle = A_{\xi}(r, \mu) \hat{r}_i \hat{r}_j + B_{\xi}(r, \mu) \delta_{ij} + C_{\xi}(r, \mu) \hat{\lambda}_i \hat{\lambda}_j + D_{\xi}(r, \mu) (\hat{r}_i \hat{\lambda}_j + \hat{r}_j \hat{\lambda}_i) \quad (1)$$

where the separation vector $\mathbf{r} = \mathbf{x}_1 - \mathbf{x}_2$ has the magnitude r and the direction specified by the unit vector $\hat{\mathbf{r}}$. The direction of the symmetry axis set by the mean magnetic field is given by the unit vector $\hat{\lambda}$ and $\mu = \hat{\mathbf{r}} \cdot \hat{\lambda}$. The magnetic field correlation tensor may also have antisymmetric, helical part, however it does not contribute to synchrotron correlations. Hence, further on we shall consider only the index-symmetric part of $\langle H_i(\mathbf{x}_1) H_j(\mathbf{x}_2) \rangle$.

The structure function of the field has the same representation

$$\frac{1}{2} \langle (H_i(\mathbf{x}_1) - H_i(\mathbf{x}_2)) (H_j(\mathbf{x}_1) - H_j(\mathbf{x}_2)) \rangle = A(r, \mu) \hat{r}_i \hat{r}_j + B(r, \mu) \delta_{ij} + C(r, \mu) \hat{\lambda}_i \hat{\lambda}_j + D(r, \mu) (\hat{r}_i \hat{\lambda}_j + \hat{r}_j \hat{\lambda}_i) \quad (2)$$

with coefficients $A(r, \mu) = A_{\xi}(0, \mu) - A_{\xi}(r, \mu)$, ... etc. In case of power-law spectra, one can use either the correlation function or the structure function, depending on the spectral slope. In this case the structure function coefficients can be thought of as renormalized correlation coefficients.

¹ The original GS95 model was formulated in terms of global system of reference and used closure relations which are only valid in this system of reference. This point was corrected in further publications (Lazarian & Vishniac 1999; Cho & Vishniac 2000; Maron & Goldreich 2001; Cho et al. 2002) where the necessity of using local reference system defined by magnetic field on the scale of turbulence study was suggested, justified and tested. When in the literature the critical balance and the relation between parallel and perpendicular scales are still expressed in terms of parallel and perpendicular wavenumbers, the corresponding wavenumbers should be understood as shorthand notations of the inverse scales calculated in the local reference frame, rather than wavenumbers in the system of reference related to the mean magnetic field.

² Recent debates, for instance, were centered on the role of dynamical alignment or polarization intermittency that could change the slope of MHD turbulence from the Kolmogorov slope predicted in the GS95 to a more shallow slope observed in numerical simulations (see Boldyrev 2005, 2006; Beresnyak & Lazarian 2006). More recent studies (see Beresnyak & Lazarian 2009, 2010) indicate that numerical simulations may not have enough dynamical range to test the actual spectrum of turbulence and the flattening of the spectrum measured in the numerical simulations is expected due to MHD turbulence being less local than its hydro counterpart.

In Appendix B we discuss the relation of the correlation tensor and spectrum tensor representation of the axisymmetric turbulent fields. An observer studying synchrotron does not map projected magnetic fluctuations directly, as the synchrotron emission is a non-linear function of the magnetic field component perpendicular to the line of sight. This is the subject of the next section.

3. 3D SPATIAL CORRELATIONS OF SYNCHROTRON EMISSIVITY

The goal of this section is to show that one can introduce measures of synchrotron correlation which very weakly depend on the electron spectral distribution, i.e. on γ . Whenever possible we provide the prove analytically for selected cases. We also show results of numerical calculations.

3.1. Synchrotron correlations

Synchrotron emission arises from relativistic electron spiraling about magnetic fields. The emission has been discussed in many monographs (see Pacholczyk 1970, Fleishman 2008, and references therein). Careful study of the formation of the synchrotron signal (see Westfold 1959) revealed that the signal is *essentially* non-linear in the magnetic field H (B). The origin of nonlinearity is in relativistic effects. Nonlinearity comes from the fact that the signal is formed only over the narrow fraction of the electron cycle, and the two leading orders in the deviation of the trajectory from the straight line give the same contribution in terms of $1/\gamma$. Summation of the result over “flashes” is also non-straightforward, and produces spread frequency spectrum (Westfold 1959). Situation is remarkably different from cyclotron (non relativistic) emission where emission is monochromatic and has intensity just quadratic in the magnetic field.

If the distribution of relativistic electrons is

$$N_e(\mathcal{E})d\mathcal{E} \sim \mathcal{E}^\alpha d\mathcal{E} \quad (3)$$

then the observer sees intensity of the synchrotron emission is, thus,

$$I_{sync}(\mathbf{X}) \propto \int dz H_\perp^\gamma(\mathbf{x}) \quad (4)$$

where $\mathbf{X} = (x, y)$ is the 2D position vector on the sky and $H_\perp = \sqrt{H_x^2 + H_y^2}$ is the magnitude of the magnetic field perpendicular to the line-of-sight z . Note that $\gamma = \frac{1}{2}(\alpha + 1)$ is, generally, a fractional power.

The relativistic electron power law index α changes from object to object and also varies with energy of electrons. For galactic radio halo tested at meter wavelengths, observations indicate that $\alpha \approx 2.7$ (see Pohl 1996). The index α and therefore γ may vary due to processes of acceleration and losses. In the simplest models of shock acceleration $\alpha = 2$ (see Longair 2011) and in the acceleration in turbulent reconnection $\alpha = 2.5$ (see de Gouveia dal Pino & Lazarian 2005). Those should produce $\gamma = 1.5$ and $\gamma = 1.75$, respectively. In reality, the acceleration of particles is a more sophisticated process which in case of a shock includes the formation of the precursor and its interaction with the media (see Beresnyak et al. 2009; Malkov & Diamond 2009) as well as various feedback processes. As a result of these and propagation effects γ will vary. In this paper we consider variations of γ in the range from 1 to 4, which covers the astrophysically important cases we are aware of.

In observations, one measures the correlation function of the synchrotron intensity

$$\xi_{sync}(\mathbf{R}) \equiv \langle I_{sync}(\mathbf{X}_1) I_{sync}(\mathbf{X}_2) \rangle \propto \int dz_1 dz_2 \langle H_\perp^\gamma(\mathbf{x}_1) H_\perp^\gamma(\mathbf{x}_2) \rangle \quad (5)$$

by averaging over an ensemble of the pairs of the sky measurements at fixed two dimensional separation $\mathbf{R} = \mathbf{X}_1 - \mathbf{X}_2$. This function is the projection of the three-dimensional correlation of emissivity

$$\xi_{H_\perp^\gamma}(\mathbf{R}, z) = \langle H_\perp^\gamma(\mathbf{x}_1) H_\perp^\gamma(\mathbf{x}_2) \rangle \quad (6)$$

which for homogeneous turbulence depends only on $\mathbf{x}_1 - \mathbf{x}_2 = (\mathbf{R}, z)$.

The structure function is formally related to the correlation one

$$D_{sync}(\mathbf{R}) \equiv \langle (I_{sync}(\mathbf{X}_1) - I_{sync}(\mathbf{X}_2))^2 \rangle \propto 2 \int dz_1 \int dz \left(\xi_{H_\perp^\gamma}(0, z) - \xi_{H_\perp^\gamma}(\mathbf{R}, z) \right) \quad (7)$$

but it can often be defined even when the correlation function itself has a divergent behaviour.

Thus, we are presented with the problem of describing the correlation between the fractional powers of the magnitudes of the orthogonal projections of a vector field, $\xi_{H_\perp^\gamma}$. Our main aim is to demonstrate that one can develop statistical measures that are insensitive to the parameter γ . Using these statistics simplifies the interpretation of the observational signal in terms of the properties of the magnetized turbulence.

Our approach is the following. Let us note that however complex the statistics of the magnetic field is, the observed correlations are functions of just three functional quantities, $\xi_{xx}(\mathbf{r}) = \langle H_x(\mathbf{x}_1) H_x(\mathbf{x}_2) \rangle$, $\xi_{yy}(\mathbf{r}) = \langle H_y(\mathbf{x}_1) H_y(\mathbf{x}_2) \rangle$ and $\xi_{xy}(\mathbf{r}) = \langle H_x(\mathbf{x}_1) H_y(\mathbf{x}_2) \rangle$. To study the γ dependence of the correlation of emissivity $\xi_{H_\perp^\gamma}$, we shall consider it in the space spanned by $\xi_{xx}, \xi_{yy}, \xi_{xy}$ as independent variables, $\xi_{H_\perp^\gamma}(\xi_{xx}, \xi_{yy}, \xi_{xy})$.

3.2. Statistically isotropic magnetic field and synchrotron correlations

First we consider the case when statistics of the magnetic field is isotropic, which may, for instance, correspond to the super-Alfvénic turbulence, i.e. for the turbulence with the injection velocity much in excess of the Alfvénic one. The structure tensor of a Gaussian isotropic vector field, a special case of Eq. (2), is usually written in the form

$$\langle (H_i(\mathbf{x}_1) - H_i(\mathbf{x}_2)) (H_j(\mathbf{x}_1) - H_j(\mathbf{x}_2)) \rangle = (D_{LL} - D_{NN}) \hat{r}_i \hat{r}_j + D_{NN} \delta_{ij} \quad , \quad (8)$$

where $D_{LL}(r)$ and $D_{NN}(r)$ are structure functions that describe, respectively, the correlation of the vector components parallel and orthogonal to point separation \mathbf{r} . In case of solenoidal vector field, in particular the magnetic field, two structure functions are related by

$$\frac{d}{dr} D_{LL} = -\frac{2}{r} (D_{LL} - D_{NN}) \quad (9)$$

which in the regime of the power-law behaviour $D_{NN} \propto r^m$ leads to both functions being proportional to each other $D_{LL} = \frac{2}{2+m} D_{NN}$.

To describe our system we chose the x-axis to coincide with the direction of the projected separation \mathbf{R} . This can be done for analysis of isotropic statistics since there is no other preferred direction. In this case, we find the following two correlations

$$d_1 \equiv \langle [H_x(\mathbf{X}_1, z_1) - H_x(\mathbf{X}_2, z_2)]^2 \rangle = (D_{LL} - D_{NN}) \sin^2 \theta + D_{NN} \quad (10)$$

$$d_2 \equiv \langle [H_y(\mathbf{X}_1, z_1) - H_y(\mathbf{X}_2, z_2)]^2 \rangle = D_{NN} \quad (11)$$

$$\langle [H_x(\mathbf{X}_1, z_1) - H_y(\mathbf{X}_2, z_2)]^2 \rangle = 0 \quad (12)$$

to determine completely the correlations of the orthogonal components of the magnetic field. Here θ is the angle between the 3D separation vector \mathbf{r} and the line of sight.

For convenience we shall also introduce the normalized correlation coefficients

$$c_1 \equiv \langle H_x(\mathbf{X}_1, z_1) H_x(\mathbf{X}_2, z_2) \rangle / \langle H_x(\mathbf{X}_1, z_1)^2 \rangle = 1 - \frac{1}{2} d_1 \quad (13)$$

$$c_2 \equiv \langle H_y(\mathbf{X}_1, z_1) H_y(\mathbf{X}_2, z_2) \rangle / \langle H_y(\mathbf{X}_1, z_1)^2 \rangle = 1 - \frac{1}{2} d_2 \quad (14)$$

which vary from unity for coincident points to zero at large separation. Normalized structure functions, conversely, are zero at small separations and reach asymptotically the value of two where the correlation vanishes.

Let us now investigate the *normalized* correlations

$$\tilde{\xi}_{H_\perp^\gamma} = \left(\langle H_\perp^\gamma(\mathbf{x}_1) H_\perp^\gamma(\mathbf{x}_2) \rangle - \langle H_\perp^\gamma(\mathbf{x}) \rangle^2 \right) / \left(\langle H_\perp^\gamma(\mathbf{x})^2 \rangle - \langle H_\perp^\gamma(\mathbf{x}) \rangle^2 \right) \quad (15)$$

$$\tilde{D}_{H_\perp^\gamma} = 2 \left(1 - \tilde{\xi}_{H_\perp^\gamma} \right) \quad (16)$$

where the mean and the variance can be trivially expressed through Gamma functions

$$\langle H_\perp^\gamma(\mathbf{x}) \rangle = 2^{\gamma/2} \Gamma[1 + \gamma/2] H^\gamma \quad (17)$$

$$\langle H_\perp^\gamma(\mathbf{x})^2 \rangle = 2^\gamma \Gamma[1 + \gamma] H^{2\gamma} \quad (18)$$

where H is the amplitude of the magnetic field. Both the mean $\langle H_\perp^\gamma(\mathbf{x}) \rangle$ and the variance $\langle H_\perp^\gamma(\mathbf{x})^2 \rangle - \langle H_\perp^\gamma(\mathbf{x}) \rangle^2$ that determine the average intensity and the rms fluctuations of the synchrotron emission are strong functions of γ index. However, as we shall demonstrate, the normalized correlation is not, thus providing a direct measure to the correlation properties of the magnetic field.

Below we identify the normalized correlations of synchrotron emission as the measures which depend on the index γ only weakly. The goal is to reduce the problem of relating magnetic field and synchrotron statistics for an arbitrary γ to the mathematically trackable case of $\gamma = 2$.

3.2.1. Special cases of spectral index: $\gamma = 2$ and 4

In case of even integer γ , among which of the most interest are cases $\gamma = 2$ and $\gamma = 4$, the correlation of the emissivity can be found analytically to yield

$$\tilde{\xi}_{H_\perp^2} = \frac{1}{2} (c_1^2 + c_2^2) \quad \gamma = 2 \quad (19)$$

$$\tilde{\xi}_{H_\perp^4} = \frac{2}{5} (c_1^2 + c_2^2) + \frac{3}{40} (c_1^4 + c_2^4) + \frac{1}{20} c_1^2 c_2^2 \quad \gamma = 4 \quad (20)$$

Starting at unity when $c_1 = c_2 = 1$, the correlations show remarkably little difference throughout the whole range of c_1 and c_2 , although $\xi_{H_\perp^4} \sim \frac{4}{5} \xi_{H_\perp^2}$ as $c_1 \rightarrow 0, c_2 \rightarrow 0$.

In terms of the structure functions

$$\tilde{D}_{H\perp}^2 = (d_1 + d_2) - \frac{1}{4} (d_1^2 + d_2^2) \quad \gamma = 2 \quad (21)$$

$$\tilde{D}_{H\perp}^4 = \frac{6}{5} (d_1 + d_2) - \frac{1}{20} (d_1 + d_2)^2 \dots \quad \gamma = 4 \quad (22)$$

Although a different index leads to a change of the amplitude at small separation where linear term dominates by a factor 6/5 it does not affect the slope, and as we shall see numerically the difference in the transition to non-linear terms will be difficult to observe.

3.2.2. Case of equal correlation coefficients $c_1 = c_2$

Another special test case that can be treated analytically is the case of equal correlation between normal components and correlation of longitudinal components. In this case, for arbitrary γ

$$\xi_{H\perp}^\gamma(c_2 = c_1) = \frac{1 - {}_2F_1\left[-\frac{\gamma}{2}, -\frac{\gamma}{2}, 1, c_1^2\right]}{1 - \Gamma[1 + \gamma]\Gamma[1 + \gamma/2]^{-2}} \quad (23)$$

where ${}_2F_1\left[-\frac{\gamma}{2}\right]$ is the hypergeometric function (see Abramovitz & Stegun 1965). As the Figure 1 shows, this result is also nearly γ independent for $\gamma \in (1.5, 3)$, and with only minor differences showing only for $\gamma > 3$

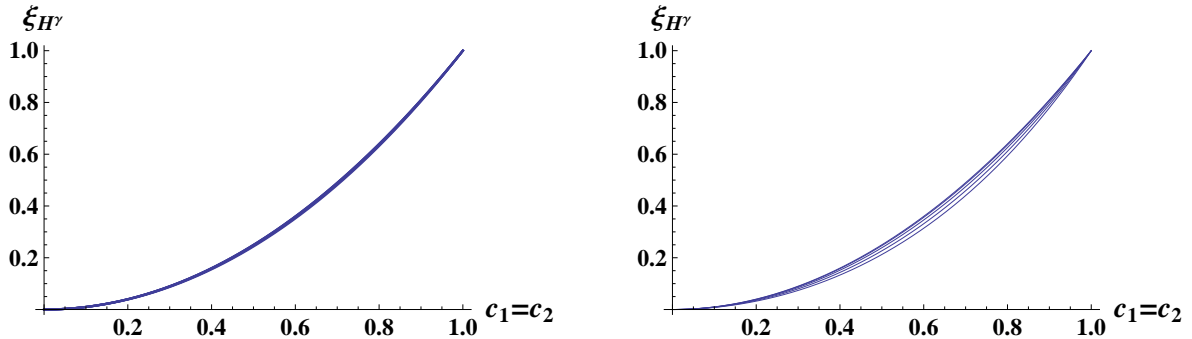


FIG. 1.— Correlation coefficients $\xi_{H\perp}^\gamma(c_1)$ for coincident $c_1 = c_2$ for several $\gamma \in (1.5, 2.8)$ (left) and $\gamma \in (2.5, 4)$ (right).

3.2.3. Conjecture of γ independence

Based on the test cases above we conjecture that the *normalized* correlation function of the synchrotron is insensitive to the γ -parameter in the range of our interest. To test this conjecture we compute numerically $\xi_{H\perp}^\gamma$ for non-integer γ 's. The results presented in Figure 2 confirm insensitivity to γ in all the range of interest. The maximal deviation in

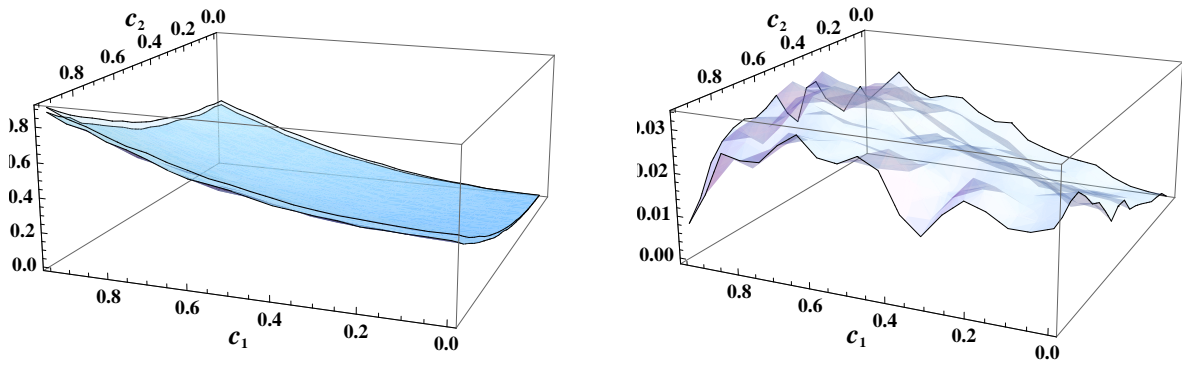


FIG. 2.— Left: Example comparison of the correlation coefficients $\xi_{H\perp}^\gamma$ for $\gamma = 2$ (top surface) and $\gamma = 3.5$ (bottom surface). Right: The difference between two surfaces in the left panel. The systematic separation between those two quite distinct cases is below 5%. Random features at 1-2% level are due to limitations of numerical integration.

correlations are limited to 3% for γ in the wide range $\gamma \in (1.2, 3)$, while staying within 10% for $\gamma = 4$.

Consequently, we conclude that the isotropic correlation of 3D synchrotron emissivity can be well approximated by a simple quadratic result of $\gamma = 2$

$$\tilde{\xi}_{H\perp}^\gamma \approx \frac{1}{2} (c_1^2 + c_2^2) \quad (24)$$

$$\tilde{D}_{H\perp}^\gamma \approx (d_1 + d_2) - \frac{1}{4} (d_1^2 + d_2^2) \quad (25)$$

In other words, while the intensity of emission changes appreciably, the correlation properties of the normalized intensities depend on γ only weakly. It is important to note that while the mapping from the magnetic field to synchrotron emissivity statistics is essentially non-linear in terms of correlation function, it is linear at small scales if the structure functions are used. That makes a structure function the preferable statistics to apply. The effects of γ manifests itself in an amplitude shift of the small scale scaling, an effect difficult to observe without very wide dynamical range.

3.3. Example of statistically anisotropic signal

While correlation properties of synchrotron emission in statistically isotropic magnetic field are described with two functions, in general, full description requires three function D_{xx} , D_{yy} and D_{xy} . Study of emission from axisymmetric turbulence belongs to this general case.

Here we shall consider the synchrotron emission in the limit when the anisotropy can be expected to play the largest role. This is the limit when a) the symmetry axis is orthogonal to the line-of-sight and b) the field has no variations in the direction of the symmetry axis. If we chose x-direction to coincide with the axis of symmetry (z-direction is along the line of sight) in this limit

$$\begin{aligned} \sigma_{xx} &= 0, & \sigma_{xy} &= 0, & \sigma_{yy} &= \sigma \\ D_{xx} &= 0, & D_{xy} &= 0, & D_{yy} &= \sigma^2 d, \end{aligned} \quad (26)$$

i.e. the correlations are described just by a single function d . Such a case has physical significance when the axis of symmetry is associated with a regular component of magnetic field, so realistic model should include non-zero mean field in x-direction, $\langle H_x \rangle \neq 0$. Perpendicular to the line of sight component of the magnetic field now has a random, y and regular, x components, $H_\perp^2 = H_y^2 + \langle H_x \rangle^2$.

The 3D emissivity of the synchrotron is correlated according to

$$\xi_{H\perp}^\gamma = \left\langle (H_y^2(\mathbf{r}_1) + \langle H_x \rangle^2)^{\gamma/2} (H_y^2(\mathbf{r}_2) + \langle H_x \rangle^2)^{\gamma/2} \right\rangle - \left\langle (H_y^2 + \langle H_x \rangle^2)^\gamma \right\rangle \quad (27)$$

which is readily computed for $\gamma = 2$ and $\gamma = 4$

$$\tilde{\xi}_{H\perp}^2 = c^2, \quad \gamma = 2 \quad (28)$$

$$\tilde{\xi}_{H\perp}^4 = c^2 \left(1 - \frac{3(\sigma^4 - c^2)}{\langle H_x \rangle^4 + 6\langle H_x \rangle^2 \sigma^2 + 12\sigma^4} \right), \quad \gamma = 4 \quad (29)$$

where c is a normalized correlation function of the magnetic field fluctuations perpendicular to the regular component of magnetic field. We find that the correlation properties of the synchrotron do not depend at all on the amplitude of the regular magnetic component if $\gamma = 2$. The left panel in Figure 3 demonstrates for $\gamma = 4$ that the difference from simple $\gamma = 2$ result decreases quickly with the strength of the regular field. Between these two cases, the correlation differ by no more than 2% along all the range of values when $\langle H_x \rangle > 3\sigma$. Similarly, for all intermediate values of γ , $\gamma = 2$ formula (28) provide the limiting behaviour when regular magnetic component is increased.

Thus, we conclude that γ dependence of normalized correlations is very weak for anisotropic turbulence in the presence of the notable regular magnetic field component. With good precision the result can be approximated by $\gamma = 2$ formula $\xi_{H\perp}^2 = \langle H_y(\mathbf{r}_1) H_y(\mathbf{r}_2) \rangle^2$.

The strongest sensitivity to γ is expected when the regular component is small, $\langle H_x \rangle \ll \sigma$. While the case of strictly one-dimensional $\langle H_x \rangle = 0$, $\langle H_x \rangle^2 = 0$ turbulent magnetic field is probably of little astrophysical importance, it provides a useful, mathematically tractable limit, of strongly anisotropic turbulence. In this limit

$$\langle H_\perp^\gamma \rangle = \frac{2^{\gamma/2} \sigma^\gamma \Gamma[\frac{1+\gamma}{2}]}{\sqrt{\pi}}, \quad \langle (H_\perp^\gamma)^2 \rangle = \frac{2^\gamma \sigma^{2\gamma} \Gamma[\frac{1}{2} + \gamma]}{\sqrt{\pi}} \quad (30)$$

$$\tilde{\xi}_{H\perp}^\gamma = \frac{{}_2F_1[-\frac{\gamma}{2}, -\frac{\gamma}{2}, \frac{1}{2}, c^2] - 1}{\sqrt{\pi} \Gamma[\frac{1}{2} + \gamma] \Gamma[\frac{1+\gamma}{2}]^{-2} - 1} \quad (31)$$

$$\tilde{D}_{H\perp}^\gamma = \frac{\sqrt{\pi} \Gamma[\frac{1}{2} + \gamma] - \Gamma[\frac{1+\gamma}{2}]^2 {}_2F_1[-\frac{\gamma}{2}, -\frac{\gamma}{2}, \frac{1}{2}, c^2]}{\sqrt{\pi} \Gamma[\frac{1}{2} + \gamma] - \Gamma[\frac{1+\gamma}{2}]^2} \quad (32)$$

The right panel in Figure 3 shows how mapping from the magnetic field to emissivity correlations behave in this limit. The $\gamma = 2$ amplitude-independent curve provides the upper bound for both $\gamma < 2$ and $\gamma > 2$ models.

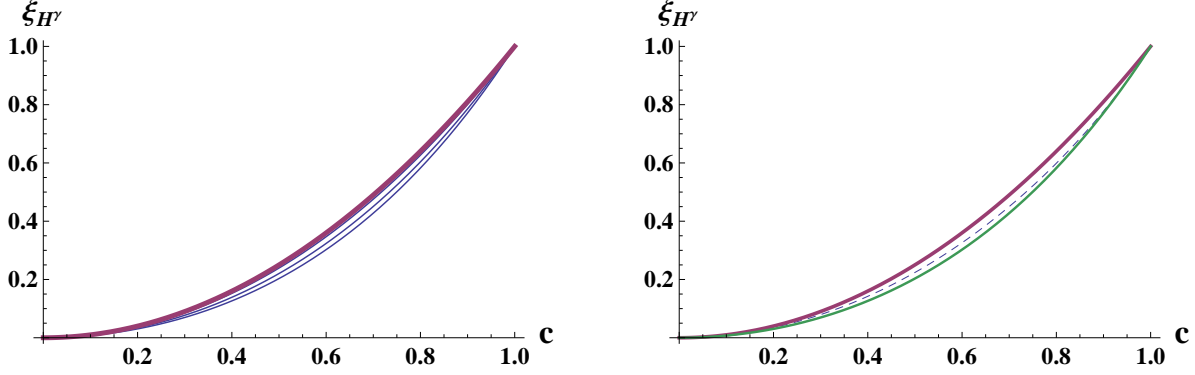


FIG. 3.— Left: correlation coefficients $\xi_{H^4}(c)$ for $\gamma = 4$ model in strongly anisotropic turbulence with varying strength of the magnitude of the regular component of the magnetic field (dashed curves starting for the lowest one at $A = 0$). The correlation approaches the $\gamma = 2$ (solid) curve as $\langle H_x \rangle$ increases beyond the rms of the random component $\langle H_y^2 \rangle^{1/2}$. Right: γ -dependence in the limit of anisotropic turbulence with absent mean field $A = 0$. The upper curve is $\gamma = 2$ case, same as on the right, the dashed curve corresponds to $\gamma = 1$ and the bottom solid one to $\gamma = 4$.

3.4. 2D correlations of synchrotron intensity in isotropic turbulence and γ dependence

Integration of the synchrotron emissivity along the line of sight provides the observer with the intensity of the emission. To demonstrate that it does not modify our conjecture of weak sensitivity to γ , we perform a detailed study of $\gamma = 2$ and $\gamma = 4$ isotropic models.

Line-of-sight projection inevitably includes correlation between widely separated regions of space. Thus one needs a statistical model of the magnetic field that is self-consistent at large separations. In physical environment the scaling of the turbulence regime can not extend to arbitrary large scales and is expected to saturate at the scales associated with energy injection r_I or the size of the turbulent region. We shall consider a simple prescription for the structure function of normal components

$$D_{NN}(r) = D(\infty) \left(\frac{r^2}{r^2 + r_I^2} \right)^{m/2} \quad (33)$$

which follows the power-law scaling $\propto r^m$ at small scales and saturates at large separations at the value equal twice the variance of the field component $D(\infty) = 2 \langle H_i^2 \rangle$. To satisfy the solenoidality condition of Eq. (9) the longitudinal structure function is

$$D_{LL}(r) = \frac{D(\infty)}{1 + m/2} \left(\frac{r}{r_I} \right)^m {}_2F_1 \left(1 + \frac{m}{2}, \frac{m}{2}, 2 + \frac{m}{2}, - \left(\frac{r}{r_I} \right)^2 \right) \quad (34)$$

The left panel in Figure 4 shows the resulting structure functions of synchrotron intensity on the sky in this isotropic

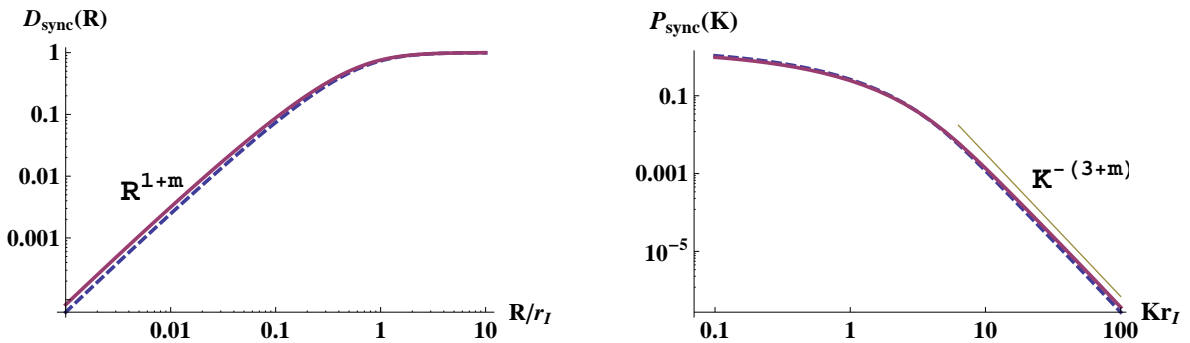


FIG. 4.— The structure functions of synchrotron intensity (left) and the power spectrum (right) in the model of isotropic Kolmogorov magnetized turbulence with $\gamma = 2$ (dashed) and $\gamma = 4$ indexes. The curves correspond to $m = 2/3$.

model for $\gamma = 2$ and $\gamma = 4$. While equal at large separations, two cases show small functional difference in the transitional regime where effects of non-linear mapping between the magnetic field and synchrotron manifest themselves. As the result, the small-scale amplitudes, where the synchrotron structure function essentially linearly reflects the magnetic field structure function, differ for $\gamma = 2$ and $\gamma = 4$ by the constant factor $\sim 6/5$, in accordance with Eq. (22). Such constant factor, however, is not readily observable if synchrotron correlations are mapped over small scales only. It is essential to track the behaviour beyond the scaling regime through non-linear transition to large scales. This encounters the following issue - the nonlinear, γ sensitive, response of the synchrotron takes place where $d \propto D_{NN}/D(\infty) \sim 1$, i.e close to energy injection scale r_I . Thus, to map it with accuracy sufficient to separate the different γ cases, would require an accurate modeling of the largest scales of the turbulent cascade.

The right panel in Figure 4 demonstrates the power spectrum that corresponds to the structure functions in the left panel. The power spectrum for $\gamma = 2$ has been studied in detail in Chepurnov (1998). The nonlinear mapping from the magnetic field to synchrotron emission affects the spectrum at long waves $Kr_I < 10$, proportional to the scale of turbulence saturation. The short scale asymptotics $\propto K^{-(3+m)}$ follows the linearized relation between magnetic field and synchrotron statistics, with only the amplitude but not the slope being weakly dependent on γ .

3.5. Correlation function of intensity for arbitrary γ

The investigation in this section allows us to approximate the emissivity correlations by the ansatz

$$\xi_{H_\perp}^\gamma(\mathbf{r}) \approx \mathcal{P}(\gamma)\xi_{H_\perp}^2(\mathbf{r}), \quad D_{H_\perp}^\gamma(\mathbf{r}) \approx \mathcal{A}(\gamma)\mathcal{P}(\gamma)D_{H_\perp}^2(\mathbf{r}), \quad (35)$$

where the strongly dependent on γ amplitude $\mathcal{P}(\gamma) \equiv \frac{\langle (H_\perp^\gamma)^2 \rangle - \langle H_\perp^\gamma \rangle^2}{\langle H_\perp^4 \rangle - \langle H_\perp^2 \rangle^2}$ is factorized from the scaling and angular dependences described by $\gamma = 2$ term. For the structure function, adjusting the amplitude in a weakly γ -dependent fashion with $\mathcal{A}(\gamma) \sim 1$ makes the approximation even more accurate at small scales.

This ansatz translates to the observable structure function of the synchrotron radiation

$$D_{sync,\gamma}(\mathbf{R}) \approx \mathcal{A}(\gamma)\mathcal{P}(\gamma)D_{sync,\gamma=2}(\mathbf{R}) \quad (36)$$

according to which the scaling and angular dependence of the synchrotron structure function can be understood from studying $\gamma = 2$ case. For isotropic magnetic fields the above expression can be rewritten using Eq. (18)

$$D_{sync,\gamma}(\mathbf{R}) \approx \mathcal{A}(\gamma)2^{\gamma-2}H^{2\gamma-4} \left(\Gamma[1+\gamma] - \Gamma\left[1+\frac{1}{2}\gamma\right]^2 \right) D_{sync,\gamma=2}(\mathbf{R}) \quad (37)$$

In case of axisymmetric turbulence one can choose the x coordinate to be aligned with the sky projection of the symmetry axis. In this frame covariance of the components of the magnetic field is diagonal, $\sigma_{xy} = 0$ and the ratio of the variances $P(\gamma)$ can be expressed via $\sigma^2 = \sigma_{xx} + \sigma_{yy}$ and $\epsilon \equiv \frac{\sigma_{xx} - \sigma_{yy}}{\sigma_{xx} + \sigma_{yy}}$ to give

$$D_{sync,\gamma}(\mathbf{R}) \approx \mathcal{A}(\gamma)\sigma^{2\gamma-4}D_{sync,\gamma=2}(\mathbf{R}) \times \quad (38)$$

$$\times \frac{(1-\epsilon^2)^\gamma}{1+\epsilon^2} \left[(1-\epsilon^2)^{\frac{1}{2}} \Gamma(1+\gamma) {}_2F_1\left(\frac{1}{2} + \frac{\gamma}{2}, 1 + \frac{\gamma}{2}, 1, \epsilon^2\right) - \Gamma\left(1 + \frac{\gamma}{2}\right)^2 {}_2F_1\left(\frac{1}{2} + \frac{\gamma}{4}, 1 + \frac{\gamma}{4}, 1, \epsilon^2\right) \right]$$

Eq. (39) relates the structure function of synchrotron intensity for arbitrary index of relativistic electrons, i.e. for arbitrary γ , with the structure function for synchrotron intensity fluctuations corresponding to $\gamma = 2$. The additional factors do not depend on the distance between points for which the correlation is thought, but uniformly change the amplitude of the structure function. Both γ and the ϵ can be obtained independently as (see Discussion). Further we simplify our treatment focusing on the case of $\gamma = 2$, while Eq. (39) allows us to generalize the results obtained for $\gamma = 2$ for an arbitrary index γ .

4. ANISOTROPY OF THE SYNCHROTRON INTENSITY STATISTICS

This section is focused on describing synchrotron fluctuations arising from a general model of axisymmetric anisotropic magnetic turbulence³. On very general grounds one can expect mean magnetic field to influence statistics of magnetic turbulence.

4.1. Power spectrum of the axisymmetric MHD turbulence

The axisymmetric tensors presented in §2 describe structure functions of turbulence. In terms of the spectral representation of axisymmetric turbulence a general form of the index-symmetric correlation tensor of the solenoidal vector field in the presence of a preferred direction $\hat{\lambda}$ is given by two scalar power spectra (Oughton et al. 1997)

$$\langle H_i H_j \rangle = \frac{1}{(2\pi)^3} \int d^3\mathbf{k} e^{i\mathbf{k}\cdot\mathbf{r}} \left[E(\mathbf{k}) \left(\delta_{ij} - \hat{k}_i \hat{k}_j \right) + F(\mathbf{k}) \frac{(\hat{\mathbf{k}} \cdot \hat{\lambda})^2 \hat{k}_i \hat{k}_j + \hat{\lambda}_i \hat{\lambda}_j - (\hat{\mathbf{k}} \cdot \hat{\lambda})(\hat{k}_i \hat{\lambda}_j + \hat{k}_j \hat{\lambda}_i)}{1 - (\hat{\mathbf{k}} \cdot \hat{\lambda})^2} \right]. \quad (39)$$

In the isotropic limit only E spectrum is present and is function only of the wave number, i.e. $E(k)$. For axisymmetric turbulence, $E(\mathbf{k})$ and $F(\mathbf{k})$ functions depend on the wave number and the angle $\mu = \hat{\mathbf{k}} \cdot \hat{\lambda}$ between the wave vector and the symmetry axis. The form of Eq. (39) is fully general if the statistics has a mirror symmetry in addition to the axial one⁴. The normalization of tensors is chosen such as to have angle-independent traces.

What combinations of E and F spectra correspond to independent modes is determined by the physical mechanisms of wave excitation and propagation. In the context of MHD, where the axis of symmetry is associated with the direction

³ A particular model of MHD turbulence that corresponds to numerical simulations is considered in the next section.

⁴ In the most general form two other pseudo-scalar spectra, C and H in the notation of Oughton et al. (1997), that describe correlations between toroidal and poloidal components of the magnetic field appear. Both terms are traceless and do not contribute to the rms energy of the magnetic field and are absent for axisymmetric turbulence with mirror symmetry. One of them, H , describes helical correlation resulting in index antisymmetric part of the correlation tensor which is irrelevant for synchrotron studies. We shall not consider possible contribution of the remaining C term in this paper.

(perhaps local) of the mean magnetic field, correlations due to Alfvénic modes correspond to the linear combination of “ E -type” and “ F -type” spectra with $F(k) = -E(k)$, while the slow and fast modes are described by the “ F -type” correlation tensors (Yan & Lazarian 2004, see also below).

When anisotropy is global, the scaling of power with wavenumber k and the angular dependence on μ factorizes. Limiting ourselves to the power-law scaling we shall consider

$$E(k, \mu) = A_E k^{-3-m_E} \hat{E}(\mu) \quad , \quad F(k, \mu) = A_F k^{-3-m_F} \hat{F}(\mu) \quad (40)$$

where $m = 2/3$ would correspond to Kolmogorov scaling. For example, in Alfvénic turbulence the fluctuations of the field are suppressed in the direction of the mean magnetic field, so one expects $\hat{E}(\mu)$ to disfavor $\mu = \pm 1$ direction. We normalize the angular functions to have unit monopoles in Legendre expansion, $\hat{E}(\mu) = \sum_{l=0}^{\infty} \hat{E}_l P_l(\mu)$, etc.,

$$\hat{E}_0 \equiv \frac{1}{2} \int_{-1}^1 d\mu \hat{E}(\mu) = 1, \quad \hat{F}_0 \equiv \frac{1}{2} \int_{-1}^1 d\mu \hat{F}(\mu) = 1 \quad (41)$$

In the presence of anisotropy the magnetic field components parallel and perpendicular to the symmetry axis have unequal variances, $\sigma_{\parallel}^2 \equiv \langle (\mathbf{H} \cdot \hat{\lambda})^2 \rangle \neq \frac{1}{2} \sigma_{\perp}^2 \equiv \frac{1}{2} \langle (\mathbf{H} \times \hat{\lambda})^2 \rangle$. Since $\langle (\mathbf{H} \cdot \hat{\lambda})(\mathbf{H} \times \hat{\lambda}) \rangle = 0$ due to azimuthal symmetry, σ_{\parallel}^2 and $\frac{1}{2} \sigma_{\perp}^2$ are the eigenvalues of the variance tensor $\sigma_{ij} = \langle H_i(\mathbf{x}) H_j(\mathbf{x}) \rangle$, and are given by

$$\sigma_{\parallel}^2 = \frac{P_E}{2} \int_{-1}^1 d\mu (1 - \mu^2) \hat{E}(\mu) + \frac{P_F}{2} \int_{-1}^1 d\mu (1 - \mu^2) \hat{F}(\mu) \quad (42)$$

$$\sigma_{\perp}^2 = \frac{P_E}{2} \int_{-1}^1 d\mu (1 + \mu^2) \hat{E}(\mu) + \frac{P_F}{2} \int_{-1}^1 d\mu \mu^2 \hat{F}(\mu) \quad (43)$$

where $P_{E,F} = 4\pi A_{E,F} \int k^2 dk k^{-3-m_{E,F}}$ are measures of the power in, respectively, E and F parts of the spectrum. Note that individual amplitudes can, in principle, be negative, while the conditions $P_E + P_F \geq 0$ and $4P_E + P_F \geq 0$ must hold.

The ratio of the two variances r_{σ} is constant in the case of measurement performed in the global system of reference

$$r_{\sigma} \equiv \frac{2\sigma_{\parallel}^2}{\sigma_{\perp}^2} = \frac{P_E + P_F - \frac{1}{5} (P_E \hat{E}_2 + P_F \hat{F}_2)}{P_E + \frac{1}{4} P_F + \frac{1}{10} (P_E \hat{E}_2 + P_F \hat{F}_2)} \quad (44)$$

The parameter $r_{\sigma} = 1$ in the isotropic case when $P_F = 0$ and $\hat{E}(\mu) = 1$. Values $r_{\sigma} < 1$ indicate the suppression while $r_{\sigma} > 1$ the enhancement of the variance in the component parallel to the symmetry axis. Notable anisotropic limit of interest is that of Alfvénic turbulence, where $P_F = -P_E$ and the component of the magnetic field along the mean is not perturbed, hence $\sigma_{\parallel}^2 = 0$ and $r_{\sigma} = 0$. E -type perturbations with completely suppressed waves along the mean magnetic field, $P_F = 0$, $\hat{E}(\mu) \propto \delta(\mu)$ lead to $r_{\sigma} = 2$. On the other hand, the essentially anisotropic F -type modes give $r_{\sigma} = 4$ even when the spectral function F is angle-independent.

4.2. Transition from local to global axisymmetry

In many physical situations, the preferred direction is local in nature and is only approximately maintained over the extended regions. In particular, in MHD turbulence $\hat{\lambda}$ is associated with the direction of the mean magnetic field which may and usually does change over large scales. In this paper we are interested in the possible anisotropy of the synchrotron signal due to existence of a preferred direction over extended regions of space, i.e a global effect. Such anisotropy is expected when the direction of the magnetic field has a long-range coherence, i.e $\hat{\lambda}$ can be thought of as fluctuating around the mean global direction $\hat{\lambda}_0$.

One can estimate the effect of $\hat{\lambda}$ “wandering” by averaging the tensor form of the correlations given by Eq. (39) over the distribution of $\hat{\lambda}$ around the mean $\hat{\lambda}_0$ (see wandering induced by Alfvénic turbulence in Lazarian & Vishniac 2000). Qualitatively the outcome is clear if the distribution of polar angle around $\hat{\lambda}_0$ is isotropic. Then, at every level of the variance of $\hat{\lambda}$, the axisymmetric nature of the statistics is maintained, so the correlation tensor must still possess the form (39) with global direction $\hat{\lambda}_0$ defining the symmetry axis. What changes when we average over local $\hat{\lambda}$ directions is the distribution of power between E and F components, with power shifted to isotropic E term as the variance of $\hat{\lambda}$ increases.

$$\begin{aligned} \overline{\langle H_i(\mathbf{k}) H_j^*(\mathbf{k}) \rangle} &= \overline{E(k, \hat{\mathbf{k}} \cdot \hat{\lambda}_0)} (\delta_{ij} - \hat{k}_i \hat{k}_j) + \\ &+ \overline{F(k, \hat{\mathbf{k}} \cdot \hat{\lambda}_0)} \left[W_I(\hat{\mathbf{k}} \cdot \hat{\lambda}_0, \sigma_{\lambda}) (\delta_{ij} - \hat{k}_i \hat{k}_j) + W_L(\hat{\mathbf{k}} \cdot \hat{\lambda}_0, \sigma_{\lambda}) \frac{(\hat{\mathbf{k}} \cdot \hat{\lambda}_0)^2 \hat{k}_i \hat{k}_j + \hat{\lambda}_{0i} \hat{\lambda}_{0j} - (\hat{\mathbf{k}} \cdot \hat{\lambda}_0)(\hat{k}_i \hat{\lambda}_{0j} + \hat{k}_j \hat{\lambda}_{0i})}{1 - (\hat{\mathbf{k}} \cdot \hat{\lambda}_0)^2} \right] \end{aligned} \quad (45)$$

where overline indicates the average over the cosine $\chi \equiv \hat{\lambda} \cdot \hat{\lambda}_0$. W_I and W_L are weight functions that depend on the measure of the average $\hat{\lambda}$ wandering σ_{λ} so that $W_L(\hat{\mathbf{k}} \cdot \hat{\lambda}_0, 0) = 1$ and $W_I(\hat{\mathbf{k}} \cdot \hat{\lambda}_0, 0) = W_L(\hat{\mathbf{k}} \cdot \hat{\lambda}_0, \infty) = 0$

While details of the averaging over local directions of $\hat{\lambda}$ depend on exact form of the power spectra, main effect can be demonstrated by just averaging the basic tensor forms. In particular, the averaged F -tensor (assigning $1 - (\mathbf{k} \cdot \hat{\lambda})^2$ norm to the spectral function for convenience) becomes

$$\begin{aligned} & \overline{(\hat{\mathbf{k}} \cdot \hat{\lambda})^2 \hat{k}_i \hat{k}_j + \hat{\lambda}_i \hat{\lambda}_j - (\hat{\mathbf{k}} \cdot \hat{\lambda})(\hat{k}_i \hat{\lambda}_j + \hat{k}_j \hat{\lambda}_i)} = \\ & = \frac{1}{2} (1 - \overline{\chi^2}) (\delta_{ij} - \hat{k}_i \hat{k}_j) + \frac{1}{2} (3\overline{\chi^2} - 1) \left((\hat{\mathbf{k}} \cdot \hat{\lambda}_0)^2 \hat{k}_i \hat{k}_j + \hat{\lambda}_{0i} \hat{\lambda}_{0j} - (\hat{\mathbf{k}} \cdot \hat{\lambda}_0)(\hat{k}_i \hat{\lambda}_{0j} + \hat{k}_j \hat{\lambda}_{0i}) \right). \end{aligned} \quad (46)$$

We see that wandering of the local λ , i.e. $\overline{\chi^2} \neq 1$, leads to the appearance of the isotropic tensor part and the suppression of the original F -type part. Although the exact weight functions between the parts depend on details, the structure of the transition described by Eq. 46 is general – the original tensor structure (of any form) that one starts with when $\hat{\lambda} = \hat{\lambda}_0$ disappears as $\hat{\lambda}$ gets distributed more and more isotropically, $\overline{\chi^2} \rightarrow \frac{1}{3}$, being replaced by the isotropic tensor.

To estimate the characteristic angle of the transition to isotropic tensor structure we plot in Figure 5 our model weight functions $W_I(\sigma_\lambda) = \frac{1}{2} (1 - \overline{\chi^2})$ and $W_L(\sigma_\lambda) = \frac{1}{2} (3\overline{\chi^2} - 1)$ assuming a simple distribution $P(\chi) = \frac{1}{\sigma_\lambda(1-e^{2/\sigma_\lambda})} \exp\left[\frac{\chi-1}{\sigma_\lambda}\right] d\chi$. With this parameterization, σ_λ matches very closely the mean deviation of cosine χ from unity as long as $\sigma_\lambda \lesssim 0.4$. We find that one can approximately use the local tensor structure of the correlation for

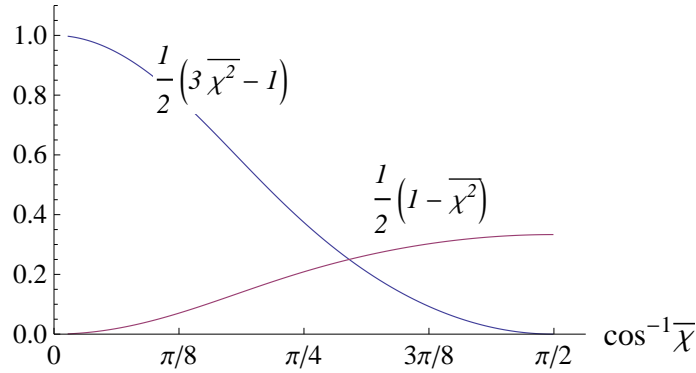


FIG. 5.— Example of the transition weights between anisotropic and isotropic correlation tensor structures as functions of the mean angle between a local and the global symmetry directions, $\cos^{-1} \bar{\chi} = \cos^{-1} (\hat{\lambda} \cdot \hat{\lambda}_0)$.

global studies when the mean deviation of $\hat{\lambda}$ from $\hat{\lambda}_0$ is less than $\pi/8$. If the mean fluctuation of $\hat{\lambda}$ exceeds $\approx 3\pi/8$, one can use the isotropic tensor. In the intermediate range $\pi/8 \lesssim \cos^{-1} \bar{\chi} \lesssim 3\pi/8$ one has a mix of the local and isotropic contributions. Two contributions are in similar proportions when $\cos^{-1} \bar{\chi} \approx \pi/4$.

The averaging in Eq. (45) is an ensemble averaging for three dimensional correlations. It worth noting that the averaging arising from field wandering in Eq. (45) acts differently on the different parts of the correlation tensor.

4.3. Structure functions at small scales

We have argued that the correlation properties of the synchrotron emission at small scales are well approximated by the linearized limit of the $\gamma = 2$ model. This allows one to study scaling properties of emission for $\gamma = 2$ and then generalize those for any astrophysically relevant γ . The full expression for the structure functional for $\gamma = 2$ (see Appendix C)

$$\begin{aligned} D_{sync}(\mathbf{R}) &= \left\langle \left[\int dz_1 H_\perp^2(\mathbf{X}_1, z_1) - \int dz_2 H_\perp^2(\mathbf{X}_2, z_2) \right]^2 \right\rangle = \\ &= \int dz_+ \int dz \{ 4\sigma_{ij} [D_{ji}(\mathbf{X}, z) - D_{ji}(0, z)] - [D_{ij}(X, z) D_{ij}(X, z) - D_{ji}(0, z) D_{ij}(0, z)] \} . \end{aligned} \quad (47)$$

in the small-scale limit (i.e. when the structure functions are much less than dispersions) provides a linearized expression

$$D_{sync}(\mathbf{R}) \sim 4\sigma_{ij} \int dz [D_{ji}(\mathbf{R}, z) - D_{ji}(0, z)] . \quad (48)$$

that involves x, y ($i, j = 1, 2$) components of the magnetic field correlation tensor.

For the following discussion we introduce the coordinate frame that has z-axis along the line-of-sight and y-axis perpendicular to the plane spanned by the line-of-sight and the symmetry axis $\hat{\lambda}$. The x-axis is then along the projection of $\hat{\lambda}$ onto the image (x, y) plane, denoted by the unit 2D vector $\hat{\Lambda}$. The vector $\hat{\lambda}$ now has components

$\hat{\lambda}_i = (\sin \theta, 0, \cos \theta)$. The polar angle of the 2D separation \mathbf{R} is denoted by ϕ while ψ is the polar angle of the 2D wave vector \mathbf{K} . Both have the meaning of angles between the correspondent vectors and $\hat{\Lambda}$.

The 2D part of the dispersion tensor σ_{ij} is diagonal in the chosen frame

$$\sigma_{xx} = \sigma_{\parallel}^2 \sin^2 \theta + \frac{1}{2} \sigma_{\perp}^2 \cos^2 \theta, \quad \sigma_{yy} = \frac{1}{2} \sigma_{\perp}^2, \quad \sigma_{xy} = 0. \quad (49)$$

Its anisotropy can be represented by the parameter

$$\epsilon \equiv \frac{\sigma_{xx} - \sigma_{yy}}{\sigma_{xx} + \sigma_{yy}} = \frac{\sin^2 \theta \left(\sigma_{\parallel}^2 - \frac{1}{2} \sigma_{\perp}^2 \right)}{\sin^2 \theta \left(\sigma_{\parallel}^2 - \frac{1}{2} \sigma_{\perp}^2 \right) + \sigma_{\perp}^2} = \frac{\sin^2 \theta (r_{\sigma} - 1)}{\sin^2 \theta (r_{\sigma} - 1) + 2} \quad (50)$$

which depends both on the properties of 3D turbulence and the projection angle θ . The parameter ϵ play a key role in interpretation of the synchrotron signal.

The integration over the line of sight is equivalent to setting $k_z = 0$ in the spectral domain. The z-axis projected correlation function of the field becomes

$$\int dz \langle H_i H_j \rangle \propto \frac{1}{(2\pi)^2} \int d^2 K e^{i\mathbf{K} \cdot \mathbf{R}} \left[E(\mathbf{K}) \left(\delta_{ij} - \hat{K}_i \hat{K}_j \right) + \sin^2 \theta F(\mathbf{K}) \frac{\cos^2 \psi \hat{K}_i \hat{K}_j + \hat{\Lambda}_i \hat{\Lambda}_j - \cos \psi (\hat{K}_i \hat{\Lambda}_j + \hat{K}_j \hat{\Lambda}_i)}{1 - \cos^2 \psi \sin^2 \theta} \right] \quad (51)$$

where, as we discussed earlier $E(\mathbf{K})$ and $F(\mathbf{K})$ functions describe the underlying statistics of turbulence.

The 2D power spectra $E(\mathbf{K}) = E(k_z = 0)$ and $F(\mathbf{K}) = F(k_z = 0)$ ⁵ depend, parametrically, on the angle θ between the symmetry axis and the line of sight. Notably, the contribution from the F -modes vanishes if the axis of symmetry is along the line-of-sight, $\sin \theta = 0$.

More interesting is the dependence on the positional angle ψ . One can deal with the harmonic decomposition of 2D spectra which is defined as $E_n(K) = \frac{1}{2\pi} \int_0^{2\pi} d\psi e^{-in\psi} E(K, \psi)$, and analogously for $F_n(K)$.

Below we obtain expressions for multipoles of the decomposition of 2D structure functions of magnetic field. These multipoles can be studied observationally. In what follows we transform back to the correlation function domain we express the spectral tensors by the differential operators. We consider separately the additive E and F contributions to the structure functions.

4.3.1. Multipole expansion for E -term

Correlation function that arises from E -type spectral tensor can be expressed as

$$\int dz \langle H_i H_j \rangle \propto (\partial_i \partial_j - \delta_{ij} \Delta) \Phi_E(R, \phi), \quad (52)$$

with

$$\Phi_E(R, \phi) \equiv \sum_{n=-\infty}^{\infty} i^n e^{in\phi} \int K^{-1} dK J_n(KR) E_n(K) \quad (53)$$

The synchrotron structure function has a similar form

$$D_{sync}(\mathbf{R}) \propto 8\sigma_{ij} (\partial_i \partial_j - \delta_{ij} \Delta) \Phi_{reg}(R, \phi) \quad (54)$$

but with the regularized $\Phi_{reg}(R, \phi) = \Phi(0, \phi) - \Phi(R, \phi)$ ⁶. It becomes

$$D_{sync}(R, \phi) \propto -(\sigma_{xx} + \sigma_{yy}) \Delta \Phi_{reg}(R, \phi) + (\sigma_{xx} - \sigma_{yy}) (\partial_x^2 - \partial_y^2) \Phi_{reg}(R, \phi). \quad (55)$$

Both terms have concise multipole expansions

$$\Delta \Phi_{reg}(R, \phi) = \sum_{n=-\infty}^{\infty} i^n e^{in\phi} \int_0^{\infty} K dK [J_n(KR) - J_n(0)] E_n \quad (56)$$

$$(\partial_x^2 - \partial_y^2) \Phi_{reg}(R, \phi) = \sum_{n=-\infty}^{\infty} i^n e^{in\phi} \int_0^{\infty} K dK [J_n(KR) - J_n(0)] \frac{E_{n+2} + E_{n-2}}{2} \quad (57)$$

that lead to the expression for the multipoles of the normalized synchrotron structure function

$$\begin{aligned} \bar{D}_n(R) &\equiv \frac{1}{2\pi} \int_0^{2\pi} d\phi e^{-in\phi} \bar{D}_{sync}(R, \phi) = \\ &= i^n \int_0^{\infty} K dK [J_n(0) - J_n(KR)] \left[E_n - \frac{1}{2} \epsilon (E_{n+2} + E_{n-2}) \right]. \end{aligned} \quad (58)$$

⁵ We shall use the same letter notation for 3D and 2D spectra, which, hopefully, should not lead to the confusion.

⁶ We have left ϕ dependence in $\Phi(0, \phi)$ to signify that regularization may affect not only the monopole but also the higher harmonics.

The first term directly maps the multipole terms of the power spectrum to correspondent multipole terms in the projected correlation function, while the second one describes the multipole coupling in the presence of anisotropy. In particular, the spectral quadrupole feeds into the monopole of the structure function

$$\tilde{D}_0(R) = \int_0^\infty K dK [1 - J_0(KR)] [E_0 - \frac{1}{2}\epsilon(E_2 + E_{-2})] , \quad (59)$$

while the quadrupole dependence of the correlation is affected by the monopole and the octupole of the spectrum

$$\tilde{D}_{\pm 2}(R) = \int_0^\infty K dK J_2(KR) [E_{\pm 2} - \frac{1}{2}\epsilon(E_0 + E_{\pm 4})] . \quad (60)$$

With factorization Eq. (40) in place, the multipole terms of the synchrotron intensity in small scale regime and $\gamma = 2$ are

$$\tilde{D}_n(R) \approx A_E C_n(m) \left(\hat{E}_n - \frac{1}{2}\epsilon \left(\hat{E}_{n+2} + \hat{E}_{n-2} \right) \right) R^{1+m} , \quad (61)$$

$$C_n(m) = -\frac{i^n \Gamma \left[\frac{1}{2}(|n| - m - 1) \right]}{2^{2+m} \Gamma \left[\frac{1}{2}(|n| + m + 3) \right]} . \quad (62)$$

The expression for the coefficients is valid for $m < 1$. For the Kolmogorov index, $m = 2/3$, $C_0(2/3) \approx 1.12$, $C_2(2/3) \approx 0.51$, $C_4(2/3) \approx -0.03$, decreasing to under 1% of the monopole value for higher n . Lower m somewhat enhances the higher multipoles, e.g. for $m = 1/2$ $C_0(1/2) \approx 0.93$, $C_2(1/2) \approx 0.40$, $C_4(1/2) \approx -0.04$, although they remain small beyond $n = 4$.

Eq. (62) relates the multipoles of correlation function that can be measured to the multipoles of the underlying power spectrum that characterizes axisymmetric turbulence. The dependence on the spectral index of turbulence enters both through R^{1+m} and through $C_n(m)$ terms given by Eq. (62).

4.3.2. Multipole expansion for F -term

Expression for the F -type correlation function is somewhat more complex due to explicit angular dependence in the spectral tensor. While it is possible to represent it as the fourth-order derivatives of a single scalar function (see Oughton et al. 1997) here we shall use the direct coordinate approach.

From Eq. (51), two relevant component correlations are

$$\begin{aligned} \int dz \langle H_x H_x \rangle &\propto \frac{\sin^2 \theta}{(2\pi)^2} \int d^2 K e^{i\mathbf{K} \cdot \mathbf{R}} F(\mathbf{K}) \frac{\sin^4 \psi}{1 - \cos^2 \psi \sin^2 \theta} \\ \int dz \langle H_y H_y \rangle &\propto \frac{\sin^2 \theta}{(2\pi)^2} \int d^2 K e^{i\mathbf{K} \cdot \mathbf{R}} F(\mathbf{K}) \frac{\cos^2 \psi \sin^2 \psi}{1 - \cos^2 \psi \sin^2 \theta} \end{aligned}$$

Combining these expressions into Eq. (48) for $\tilde{D}_{sync}(R, \phi)$ and performing multipole expansion we find that the multipole coefficients of the synchrotron structure function from waves of F -type are (compare with Eq. (58))

$$\tilde{D}_n(R) \sim i^n \sin^2 \theta \int_0^\infty K dK [J_n(0) - J_n(KR)] \sum_{p=-\infty}^\infty [F_p - \frac{1}{2}\epsilon(F_{p-2} + F_{p+2})] G_{n-p}^F \quad (63)$$

where harmonic coefficients of the angular function that describes the trace, $xx + yy$, of F -tensor (divided by $\sin^2 \theta$) is

$$G_p^F(\theta) = \frac{1}{2\pi} \int_0^{2\pi} d\psi e^{-ip\psi} \frac{\sin^2 \psi}{1 - \cos^2 \psi \sin^2 \theta} \quad (64)$$

This function describes how the spectrum contributes to different angular multipoles in the observed synchrotron correlations. It is especially important in many interesting cases when the spectrum $F(\mathbf{K})$ is isotropic, since then it determines the angular behaviour of D_{sync} in its entirety.

Geometric functions that arise in our studies are presented, in particular graphically, in Appendix D. In two limiting cases, G^F contains only low harmonics. For $\theta = 0$ ⁷, G^F contributes the monopole $G_0^F(0) = \frac{1}{2}$ and the quadrupole $G_2^F(0) = -\frac{1}{2}G_0^F(0)$ terms only, while in the opposite limit, $\theta = \frac{1}{2}\pi$, there is just the monopole $G_0^F(\pi/2) = 2G_0^F(0)$. Varying the symmetry orientation angle θ (see Figure in Appendix D) changes the power distribution between harmonics $G_p^F(\theta)$ in a rather complex way due to singular behaviour at $\theta \rightarrow \frac{1}{2}\pi$. At steep angles $\theta < \pi/3$ as symmetry axis approaches sky direction, the whole train of high multipoles is generated, albeit at decreasing amplitudes. This may or may not lead to observable consequences, especially in the context of steep spectra that suppress high multipole contributions even further.

The relation between multipoles of the observed intensity correlation function and multipoles of the underlying spectrum in case of the F -term is

$$\tilde{D}_n(R) \sim A_F C_n(m) \sin^2 \theta \sum_{p=-\infty}^\infty \left[\hat{F}_p - \frac{1}{2}\epsilon \left(\hat{F}_{p-2} + \hat{F}_{p+2} \right) \right] G_{n-p}^F R^{1+m} . \quad (65)$$

⁷ We reiterate that if the symmetry axis is along the line-of-sight this signal is not observed due to amplitude suppression from line-of-sight integration. However, this case is relevant for consideration of the fast modes in high- β MHD turbulence

5. SYNCHROTRON EMISSION FROM MHD TURBULENCE

In the previous section we dealt with a general form of the tensor of the axisymmetric solenoidal field. A realistic MHD turbulence corresponds to the particular form of this tensor. In what follows we use the model of compressible MHD turbulence that follows from numerical simulations and also can be justified theoretically. Predictions obtained within this model can be used to test the model and can provide insight into the role of compressible (fast and slow modes) versus non-compressible (Alfvén modes) motions.

5.1. Model of Alfvénic turbulence

It has been well known that small amplitude magnetic perturbations can be decomposed into Alfvén, slow and fast basic MHD modes. However, as the conventional discussion involves the decomposition in respect to the mean field, such a decomposition becomes questionable for any magnetic field perturbations of appreciable amplitude. The use of local system of reference (see Lazarian & Vishniac 1999; Cho & Vishniac 2000) makes the procedure justifiable. The *statistical* decomposition of the modes has been performed in Cho & Lazarian (2002, 2003); Kowal & Lazarian (2010). It was proven that the modes provide cascades of their own and the drainage of energy between the cascades is limited.

Alfvénic modes are the most important ones with the most of the energy residing in them and they are less subject to damping in astrophysical plasmas (see Cho & Lazarian 2002). They have the statistical properties which are similar to the Alfvénic modes obtained in incompressible simulations (Cho & Lazarian 2003). This motivates us to study the Alfvénic turbulence as our primary example.

The spectrum of Alfvénic modes was obtained in Cho et al. (2002) for the driving turbulence at large scale with V_L equal to the Alfvén velocity:

$$E(\mathbf{k}) \propto k^{-10/3} L^{-1/3} \exp \left[-\frac{k_{\parallel}}{L^{-1/3} k_{\perp}^{2/3}} \right], \quad (66)$$

where L is the injection scale of the turbulence. The exponent in Eq. (66) reflects the so-called *critical balance* condition between the parallel and perpendicular modes. It shows that most of the energy resides around the wavenumbers where the turnover of the turbulent eddies is equal to the period of the Alfvén wave.

Note that the driving at $V_L = V_A$ corresponds to model of GS95 turbulence. In the case of weaker driving at the outer scale, the turbulence becomes sub-Alfvénic at all scales and the relations between k_{\parallel} and k_{\perp} from LV99 should be used. Namely, the critical balance condition provides a modified relation between the parallel and perpendicular modes at sufficiently small scales

$$k_{\parallel} \sim L^{-1} (k_{\perp} L)^{2/3} M_A^{4/3} \quad (67)$$

where M_A is the Alfvén Mach number, which is V_L/V_A . Therefore one expects that the description of the turbulence for $M_A < 1$ involves the ratio of the left and right sides of the Eq. (67) in the exponent of Eq. (66). This would provide the description of turbulence in the *local* system of reference.

The tensor structure of Alfvén power spectrum is derived from the condition that displacement and velocity of plasma in an Alfvén wave \mathbf{k} are orthogonal to the plane spanned by the magnetic field and \mathbf{k} , $\mathbf{v}_A \propto \hat{\mathbf{k}} \times \hat{\lambda}$. Magnetic field response is given by the condition that fluctuating field is frozen,

$$H(\mathbf{k}) \propto \mathbf{k} \times (\mathbf{v} \times \hat{\lambda}) / \omega(\mathbf{k}), \quad (68)$$

where for the Alfvénic waves the frequency $\omega \propto \mathbf{k} \cdot \hat{\lambda}$. Simple algebraic manipulations then show

$$\langle H_i(\mathbf{k}) H_j^*(\mathbf{k}) \rangle_A \propto (\delta_{ij} - \hat{k}_i \hat{k}_j) - \frac{(\hat{\mathbf{k}} \cdot \hat{\lambda})^2 \hat{k}_i \hat{k}_j + \hat{\lambda}_i \hat{\lambda}_j - (\hat{\mathbf{k}} \cdot \hat{\lambda})(\hat{k}_i \hat{\lambda}_j + \hat{k}_j \hat{\lambda}_i)}{1 - (\hat{\mathbf{k}} \cdot \hat{\lambda})^2} \quad (69)$$

which in terms of the general $E - F$ decomposition (39) corresponds to $F(\mathbf{k}) = -E(\mathbf{k})$. This tensor reflects the absence of the perturbations in the magnetic field component parallel to the mean field $\hat{\lambda}$.

In the global system of reference, however, the anisotropy is scale independent and determined by the anisotropy at the outer scale. In this system of reference the tensor of magnetic perturbations can be given by

$$E(\mathbf{k}) \propto k^{-11/3} \exp \left[-M_a^{-4/3} \frac{|\hat{\mathbf{k}} \cdot \hat{\lambda}_0|}{(1 - (\hat{\mathbf{k}} \cdot \hat{\lambda}_0)^2)^{2/3}} \right], \quad (70)$$

arises from extending to global scales and $M_a \neq 1$ the phenomenological, locally anisotropic, model of Cho et al. (2002). The axis of symmetry is associated with the direction of the mean magnetic field $\hat{\lambda}_0$. The spectrum reflects the consideration that in critically balanced turbulence with $M_a < 1$ the modes with parallel to magnetic field wavenumber k_{\parallel} that exceed the critical value $\sim L^{-1/3} k_{\perp}^{2/3} M_a^{-4/3}$ are suppressed. At the injection scale L , if $k_{\parallel} \sim L$.

Following Section 4.2, the global tensor structure is a weighted mix of the local tensor of Eq. 69 and the isotropic tensor form. The $k_z = 0$ section of the spectrum becomes

$$\langle H_i(\mathbf{K}) H_j^*(\mathbf{K}) \rangle_A \propto K^{-11/3} \exp \left[-M_a^{-4/3} \frac{|\cos \psi| \sin \theta}{(1 - \cos^2 \psi \sin^2 \theta)^{2/3}} \right] \times \\ \times \left[(\delta_{ij} - \hat{K}_i \hat{K}_j) W_I + \left((\delta_{ij} - \hat{K}_i \hat{K}_j) - \sin^2 \theta \frac{\cos^2 \psi \hat{K}_i \hat{K}_j + \hat{\Lambda}_i \hat{\Lambda}_j - \cos \psi (\hat{K}_i \hat{\Lambda}_j + \hat{K}_j \hat{\Lambda}_i)}{1 - \cos^2 \psi \sin^2 \theta} \right) W_L \right]. \quad (71)$$

Now $\hat{\Lambda}$ is the projection of the global symmetry axis $\hat{\lambda}_0$ but for brevity we are omitting index '0' henceforth. We note that if the symmetry axis is strictly along the line of sight, $\sin \theta = 0$, the anisotropy effects are not observable in sky projection. Maximal anisotropic effects are observed when the symmetry axis is perpendicular to the line of sight, $\sin \theta = 1$. At small Mach numbers, parallel to the mean magnetic field modes are strongly suppressed and the turbulence is highly anisotropic. The effect is retained in sky projection, but is mitigated by $\sin \theta$.

The model Eq (71) that we use to discuss Alfvénic turbulence has two parameters - the Alfvénic Mach number M_a and the mean deviation angle $\bar{\chi}$ that gives the weights $W_L(\bar{\chi})$ and $W_I(\bar{\chi})$. On the other hand, the level of magnetic field wandering due to turbulence is itself related to the Alfvénic Mach number. High $M_a > 1$ turbulence leads to significant bending of magnetic field lines and isotropization of the observable statistics. Conversely, details of the local mode structure of the correlation tensor can be observable only in sub-Alfvénic, $M_a < 1$ regime. As the guiding model of the wandering consistent with given M_a we shall employ a rough prescription that M_a gives a tangent of the mean deviation of the local angle from the global axis, $\bar{\chi} \approx 1/\sqrt{1 + M_a^2}$. The sub-Alfvénic regime but with some isotropization may be relevant to synchrotron studies if the line-of-sight integration averages over regions with different magnetic field directions.

Asymmetry in the variance in sky components of the magnetic field in this model is shown in Figure 6. The parameter

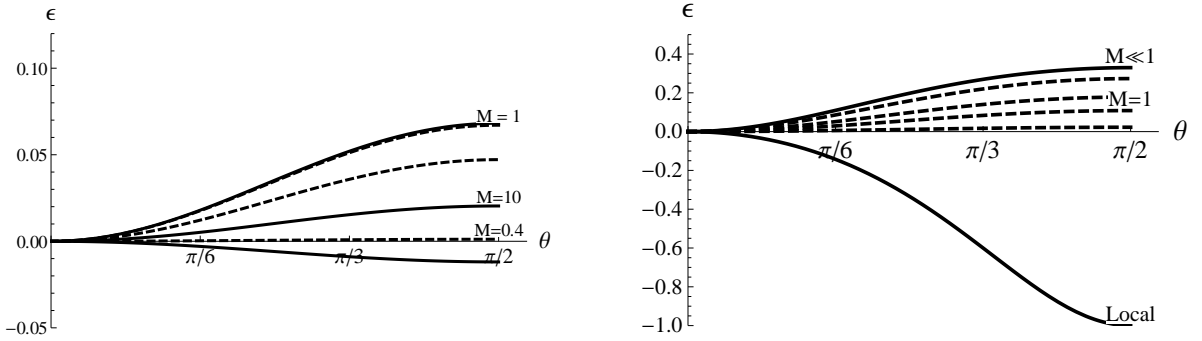


FIG. 6.— Asymmetry in the variance of the H_x (parallel to sky projection of the mean field) and perpendicular H_y , components of the magnetic field for the model of Alfvénic turbulence, Eq. (70) as parameterized by $\epsilon(\theta) = (\sigma_{xx} - \sigma_{yy})/(\sigma_{xx} + \sigma_{yy})$, as the function of the projection angle θ . Left: change from the sub-Alfvénic ($M_a = 0.1$ bottom solid) to trans-Alfvénic ($M_a \approx 1$, top solid) to super-Alfvénic ($M_a > 1$, middle solid) behaviour. Averaging over local direction of the magnetic field is carried out in accordance with M_a . Right: dependence on Mach number M_a when field wandering is neglected. The bottom solid curve in the negative sector is Mach independent result ($r_\sigma = 0$) when local tensor correlation form is assumed to hold exactly. $\epsilon > 0$ sector shows the dependence on Mach number if isotropic E -tensor (but with anisotropic $E(\mathbf{k})$) is used to model Alfvénic correlations. The dashed curves, in decreasing order of ϵ , correspond to $M_a = 0.2, 0.5, 2$. The limiting behaviour with the highest anisotropy ϵ (top solid curve marked $M_a \ll 1$) is closely followed already at $M_a \lesssim 0.2$.

ϵ , given by Eq. (50), as expected, is larger by magnitude when the symmetry axis is aligned with the sky plane, and is vanishing when it is parallel to the line of sight. Left panel shows that ϵ magnitude is small to moderate when field wandering is appropriately accounted for. ϵ is slightly negative for strongly sub-Alfvénic turbulence, almost zero at $M_a \approx 0.4$, reaches maximum positive values, $\epsilon \sim 0.1$ in trans-Alfvénic regime $M \sim 1 - 2$ and then decreases to isotropic limit $\epsilon \rightarrow 0$ for super Alfvénic M_a . However the result is somewhat sensitive on exact procedure we model the transition.

The right panel provides a cautionary illustration. If one adopts the exact local description Eq. (69) for the Alfvénic turbulence to hold through to global scales, $W_I \approx 0$, $W_L \approx 1$, then we get negative and practically M_a -independent ϵ , since $r_\sigma \approx 0$. This means that the perturbations in magnetic field component parallel to the mean field are suppressed. On the other hand, if anisotropic power spectrum is used with isotropized E -tensor form to describe the turbulence the result is opposite - parallel component is presumed to fluctuate more than the perpendicular one and $0 \leq \epsilon < 1/3$, with increasing M_a taking us to isotropic limit. Far from being just of academic interest, this latter case appear in the description of a mix of Alfvén and Slow modes in incompressible limit. We also see that averaging of the statistics over local field direction may effectively bring us to this regime, but probably not at the highest magnitude of the effect given by $r_\sigma = 2$ and $\epsilon \approx \sin^2 \theta / (\sin^2 \theta + 2)$.

In Figure 7 the distribution of power in multipoles E_n is shown for representative Alfvénic Mach numbers and several orientations θ . The multipole expansion contains only even multipoles and the real nature of coefficients reflects the presence of only the cosine terms in the decomposition. The anisotropy of the spectrum is predominately a quadrupole

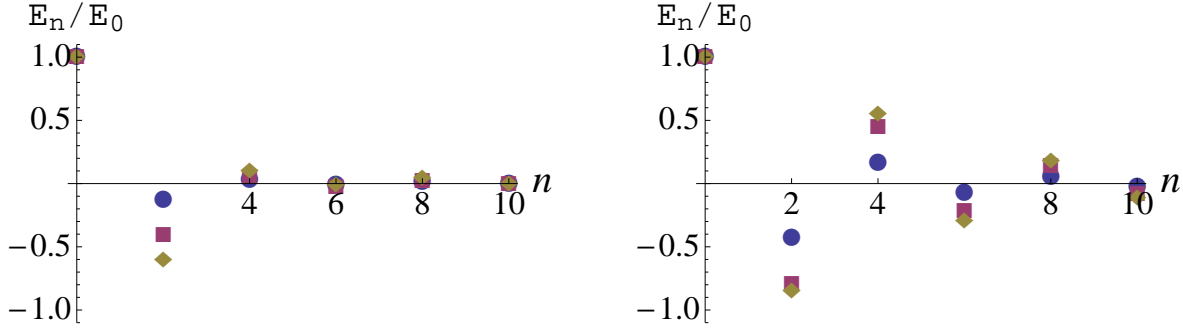


FIG. 7.— Multipole distribution of power in the units of the monopole \hat{E}_n/\hat{E}_0 for $M_a = 1$ (left) and $M_a = 0.4$ (right) for $\theta = \frac{1}{6}\pi, \frac{1}{3}\pi, \frac{1}{2}\pi$ (circles, squares and diamonds, respectively).

one for $M_a \gtrsim 1$. As M_a decreases, the higher multipoles appear and in the limit the spectrum contains all E_n of equal amplitudes with compensating alternating signs. The presence of high multipoles is largely due to sharp features in angular dependence of the spectrum which are artifacts of the model (see Cho et al. 2002, for technical remedies of this issue).

The structure function of the synchrotron fluctuations from Alfvénic modes is a special combination of Eqs. (61) and (65) that matches Eq. (71)

$$\tilde{D}_n(R) \approx A_A C_n(2/3) \left[W_I \left(\hat{E}_n - \frac{1}{2}\epsilon \left(\hat{E}_{n+2} + \hat{E}_{n-2} \right) \right) + W_L \sum_{p=-\infty}^{\infty} \left[\hat{E}_p - \frac{1}{2}\epsilon \left(\hat{E}_{p-2} + \hat{E}_{p+2} \right) \right] G_{n-p}^A \right] R^{5/3}. \quad (72)$$

where we refer to Appendix D for the properties of $G^A(\theta)$ function. In many cases Alfvénic modes are expected to dominate magnetic field perturbations and therefore Eq. (72) provides a good representation of the multipoles of the structure function of the synchrotron intensity for small 2D separations between the lines of sight $|R| \ll L$, where L is the injection scale of the turbulence⁸.

5.2. Fast modes

Fast modes are compressible modes which in high beta plasma, i.e. plasma with gaseous pressure much larger than the magnetic one, transfer to sound waves, while in low beta plasma propagate with Alfvén velocity due to compressions of the magnetic field. These modes marginally interact with Alfvén modes and were shown to form their own cascade. They were identified with an isotropic spectral function in Cho & Lazarian (2002, 2003). The tensor form of the fast mode turbulence was presented in Yan & Lazarian (2004)

$$\langle H_i(\mathbf{k}) H_j^*(\mathbf{k}) \rangle_F = \frac{k^{-7/2}}{8\pi L^{1/2}} \frac{(\hat{\mathbf{k}} \cdot \hat{\lambda})^2 \hat{k}_i \hat{k}_j + \hat{\lambda}_i \hat{\lambda}_j - (\hat{\mathbf{k}} \cdot \hat{\lambda})(\hat{k}_i \hat{\lambda}_j + \hat{k}_j \hat{\lambda}_i)}{1 - (\hat{\mathbf{k}} \cdot \hat{\lambda})^2} \times \begin{cases} 1 & (\text{low } \beta) \\ 1 - (\hat{\mathbf{k}} \cdot \hat{\lambda})^2 & (\text{high } \beta) \end{cases} \quad (73)$$

The difference between fast modes in high- β and low- β plasmas comes from different behaviour of the velocities in the medium. While by very definition of the fast modes the velocity at a wave \mathbf{k} lies in the plane spanned by \hat{k} and $\hat{\lambda}$, for $\beta \gg 1$ velocities are potential, while for $\beta \ll 1$ they are orthogonal to the direction of the magnetic field $\hat{\lambda}$. The frequency of fast modes $\omega_F(\mathbf{k})$ has a weak additional dependence on the direction of the wave vector if $\beta \sim 1$, the effect we do not consider here.

In contrast to Alfvén modes, fast modes are of F -type. Despite the isotropic power scaling, fast modes are not statistically isotropic, with anisotropy built into the tensor structure of the spectrum.

Asymmetry in the variance of the sky components of the magnetic field for fast modes is plotted in Figure 8. Compared with that of the Alfvén modes, fast modes always produce positive anisotropy ϵ . This effect is quite distinct from Alfvénic modes where ϵ is much smaller, or even negative. Determining ϵ from fitting multipole composition of synchrotron correlations may give result that distinguishes whether we are dealing with fast (positive $\epsilon > 1/3$) modes.

Isotropic nature of the power scaling leads to a very simple application of Eqs. (65) and (61) to MHD fast modes. In low β case we have $F(\mathbf{K}) \propto K^{-7/2}$ which corresponds to $m = 1/2$ and only the monopole \hat{F}_0 present. This gives

$$\tilde{D}_n(R) \sim A_F C_n(1/2) [W_I (\delta_{n0} - \epsilon \delta_{n2}) + W_L \sin^2 \theta (G_n^F(\theta) - \frac{1}{2}\epsilon [G_{n-2}^F(\theta) + G_{n+2}^F(\theta)])] \hat{F}_0 R^{3/2} \quad (\text{low } \beta) \quad (74)$$

Additional angular dependence in the spectrum in high- β medium can be accounted for by just evaluating the G_n^F coefficients at $\theta = 0$

$$\tilde{D}_n(R) \sim A_F C_n(1/2) [W_I (\delta_{n0} - \epsilon \delta_{n2}) + W_L \sin^2 \theta (G_n^F(0) - \frac{1}{2}\epsilon [G_{n-2}^F(0) + G_{n+2}^F(0)])] \hat{F}_0 R^{3/2} \quad (\text{high } \beta) \quad (75)$$

⁸ For the observed correlation functions this means that the angle $\phi \ll L/D$, where D is the distance to the object.

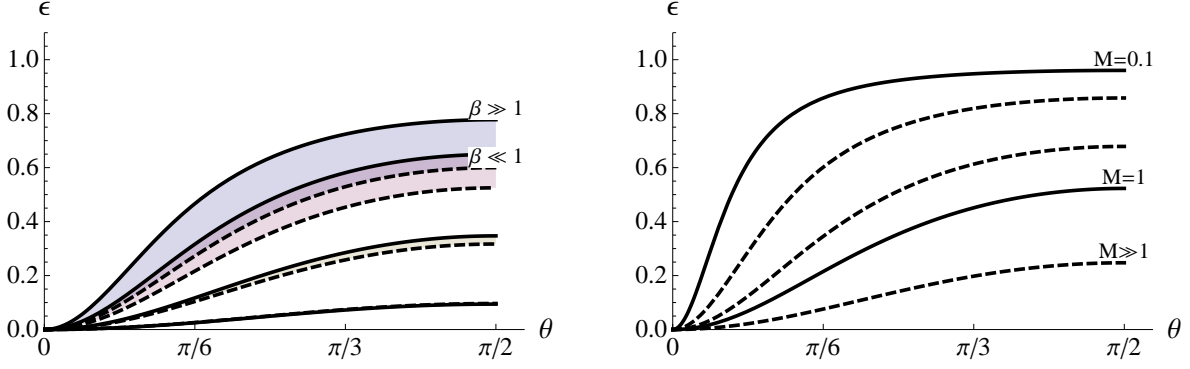


FIG. 8.— Left: $\epsilon(\theta) = (\sigma_{xx} - \sigma_{yy})/(\sigma_{xx} + \sigma_{yy})$, as the function of the projection angle θ for the fast modes. Solid lines: change in high- β plasma from the local behaviour $W_L = 1, W_I = 0$ (top) to the isotropized limit $W_L = 0$ (bottom) through intermediate cases that corresponds to average angle of local λ deviations of $\pi/8, \pi/4, 3\pi/8$ (from top to bottom). Dashed curves - same for low- β plasma. Shading covers the interval that different β will fill for the same $\cos^{-1} \bar{\chi}$. Right: same for Slow modes. Isotropization of the slow modes is treated as associated with the increase in the Alfvénic Mach number. We note that in case of high β the averaging over λ wandering is exact, so it is useful to write explicitly the set of all non-vanishing multipoles the synchrotron structure has in this limit. Taking into account the signs of $C_n(1/2)$ coefficients we have

$$\begin{aligned}\tilde{D}_0(R) &\propto \left(W_I + \left(1 + \frac{1}{2}\epsilon\right) \frac{W_L}{2} \sin^2 \theta \right) R^{3/2} \\ \tilde{D}_2(R) &\propto - \left(\epsilon W_I + (1 + \epsilon) \frac{W_L}{4} \sin^2 \theta \right) R^{3/2} \quad (\text{high } \beta) \\ \tilde{D}_4(R) &\propto - \left(\epsilon \frac{W_L}{8} \sin^2 \theta \right) R^{3/2}\end{aligned}\quad (76)$$

The structure of the multipoles of correlation functions is different from that of multipoles arising from Alfvén modes, which allows one to separate them, finding the measure of media compressibility.

5.3. Slow modes

Slow modes are usually subdominant but provide an interesting case of the F -type modes but with the power spectrum that follows the Alfvénic power spectrum. Displacements in slow modes lie in $\hat{\mathbf{k}} - \hat{\lambda}$ plane and are orthogonal to the Fast mode ones. In the low β limit, the slow displacements are parallel to the magnetic field and do not lead to magnetic field perturbations. So we focus at $\beta \gg 1$ case where the slow mode motion of plasma is perpendicular to the wave vector, $v \propto \hat{\mathbf{k}} \times (\hat{\mathbf{k}} \times \hat{\lambda})$. The frequency of the slow mode in this regime is similar to that of Alfvén ones, $\omega_S \propto \mathbf{k} \cdot \lambda$. The frozen field condition gives the magnetic field correlation tensor of the F -type

$$\langle H_i(\mathbf{k}) H_j^*(\mathbf{k}) \rangle_S \sim E(\mathbf{k}) \frac{(\hat{\mathbf{k}} \cdot \hat{\lambda})^2 \hat{k}_i \hat{k}_j + \hat{\lambda}_i \hat{\lambda}_j - (\hat{\mathbf{k}} \cdot \hat{\lambda})(\hat{k}_i \hat{\lambda}_j + \hat{k}_j \hat{\lambda}_i)}{1 - (\hat{\mathbf{k}} \cdot \hat{\lambda})^2} \quad (\text{high } \beta \text{ only}). \quad (77)$$

Figure 8 shows that the anisotropy in the sky component of the magnetic field variance produced by Slow modes is similar to the Fast modes demonstrating isotropization as M_a increases. We stress, however, that ϵ is determined by all the modes excited in the medium and cannot be simply separated in individual contributions. The expression for the synchrotron structure function multipoles can be found by combination of the previous results Eq (65) and Eq. (70)

$$\tilde{D}_n(R) \approx A_S C_n(2/3) \left[W_I \left(\hat{E}_n - \frac{1}{2} \epsilon \left(\hat{E}_{n+2} + \hat{E}_{n-2} \right) \right) + W_L \sin^2 \theta \sum_{p=-\infty}^{\infty} \left[\hat{E}_p - \frac{1}{2} \epsilon \left(\hat{E}_{p-2} + \hat{E}_{p+2} \right) \right] G_{n-p}^F \right] R^{5/3}. \quad (78)$$

With slow modes being subdominant it is more relevant to study their contribution to synchrotron in combination with other modes. The largest effect the slow modes have are in $\beta \gg 1$ limit that describes, in effect, an incompressible plasma. Slow and Alfvén modes in this limit are two “linear polarizations” of a transverse displacement wave. In particular, if in strong turbulence the powers in slow and Alfvén modes are equal (Cho & Lazarian 2003), the waves are unpolarized. The correlation tensor that describes such waves is of a pure E -type

$$\langle H_i(\mathbf{k}) H_j^*(\mathbf{k}) \rangle_{A+S} \propto E(\mathbf{k}) \left(\delta_{ij} - \hat{k}_i \hat{k}_j \right) \quad (79)$$

In Appendix B we discuss the multipole structure of the 3D correlation function that corresponds to such spectra. The synchrotron correlation structure that corresponds to Eq. (79) has the following multipoles

$$\tilde{D}_n(R) \approx A_{AS} C_n(2/3) \left(\hat{E}_n - \frac{1}{2} \epsilon \left(\hat{E}_{n+2} + \hat{E}_{n-2} \right) \right) R^{5/3}, \quad (80)$$

which presents the structure different both from multipoles of Alfvén and fast modes.

5.4. Angular structure of synchrotron correlations from MHD modes

Full observed synchrotron signal reflects the combination of Alfvén, Fast and Slow modes in the proportion determined by the distribution of power between the modes. The structure function of the resulting emission can be obtained by linear combination of Eq. (72), Eq. (75) or Eq. (74), and Eq. (78). However the dependence on the underlying models is non-linear, since the anisotropy of magnetic field variance ϵ is determined by all the contributed modes at the same time.

First we observe that the Fast modes lead to different scaling of the synchrotron correlations than the Alfvén or Slow modes, $\propto R^{3/2}$ versus $\propto R^{5/3}$, respectively. Here we suggest to focus on the measurement of the anisotropy of $D(R, \phi)$ as independent from scaling signature of the contributions from different modes. Measurement of the moments of $D_n(R)/D_0(R)$ may prove more robust discriminant between the contribution modes in cases when power-law scaling is either not exact or its accuracy is affected by observational algorithms or theoretical approximations.

We first investigate the limit when only one of spectral contribution is dominant, either Alfvén (Eq. 72), or Fast (Eqs 75-74), modes, thus assuming ϵ determined by the dominant mode only. Then, as an example of a mix between modes we discuss the case Eq. (79) of strong incompressible turbulence which maintains both Slow and Alfvén modes.

Figure 9 shows the details of the quadrupole and octupole contributions for Alfvénic turbulence. Within our model of Eq. (72) the predicted quadrupole depends on the Alfvénic Mach number M_a and follows one of the curves in the left panel of Figure 9.

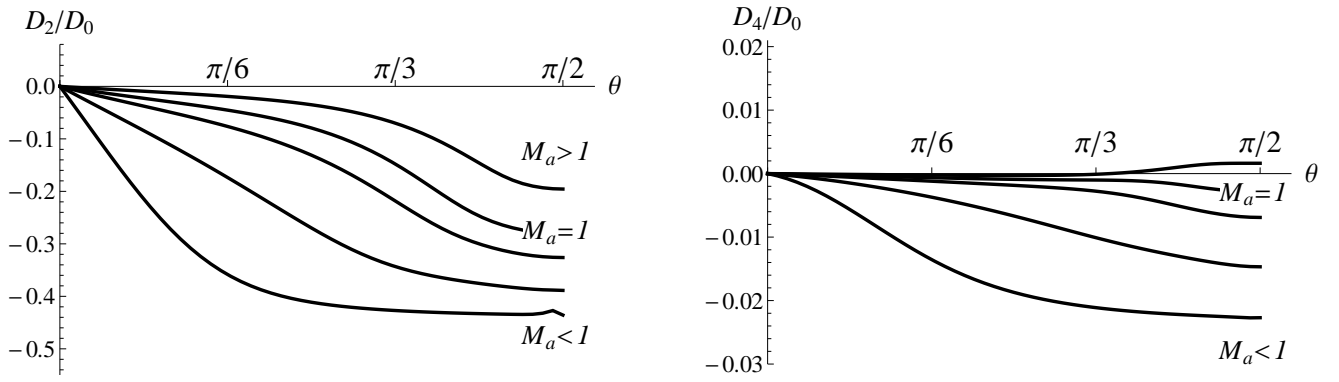


FIG. 9.— Left: Quadrupole of the synchrotron structure function in the units of the monopole versus the mean magnetic field to the line-of-sight angle θ for the Alfvén modes. Effect of Alfvénic Mach number, including expected isotropization due to fluctuations of the local field direction. The curves correspond to $M_a = 0.1, 0.4, 0.7, 1, 2$ (from lower to upper ones). Right: same plot for the octupole.

First observation from Figure 9 is that the expected quadrupole of the synchrotron correlations is *negative*. With structure functions scaling as $\sim (D_0 + D_2 \cos \phi \dots) R^{1+m}$, negative quadrupole means extended iso-correlation contours along the x-axis, the sky projected direction of the magnetic field. In case of Alfvénic turbulence this corresponds to spectral suppression of the modes parallel to the field having the dominant effect. It is easy to see from Eq. (72) that if the power distribution was 3D isotropic, the local tensor structure of the Alfvén modes would have produced a *positive* quadrupole in synchrotron, i.e the contours extended orthogonally to the symmetry axis. Thus, observing negative synchrotron quadrupole in Alfvén turbulence context is a strong argument for anisotropic underlying 3D cascade that suppresses parallel modes.

For our calculations we have adopted the model description that takes into account the fluctuations of the local direction of the magnetic field at the level determined by the M_a . Thus, changing M_a involved both the field wondering effect and the change in the power spectrum. As the result of field wondering the anisotropy of the observed synchrotron becomes suppressed when mean field is roughly aligned with the line of sight, $\theta < \pi/6$, unless the turbulence is strongly sub-Alfvénic. If field axis is closer to be orthogonal to the line of sight, the anisotropy is strong. Alfvénic turbulence leads to the negative quadrupole which magnitude is limited to $|D_2/D_0| < C_2(2/3)/C_0(2/3) = 0.45$ as M_a decreases, with values close to the limit $|D_2/D_0| \sim 0.4$ already exhibited at $M_a = 0.4$. while $|D_2/D_0| \sim 0.3$ for trans-Alfvénic $M_a \sim 1$. Measuring $D_2/D_0 \approx 0.4$ will be a strong indication of the sub Alfvénic regime. Although diminishing with higher M_a , quadrupole is still significant, $|D_2/D_0| \sim 0.1$ even for mildly super-Alfvénic $M_a \sim$ few.

Right panel in Figure 9 demonstrates that the octupole contribution is quite small, at 2% ($D_4/D_0 \sim 0.02$) level under the most favorable parameters. Indeed the steep spectra that are produced in MHD turbulence, while reflecting the multipole decomposition of the spectrum, demonstrate suppression of the multipoles higher than the quadrupole. This is the case for both Alfvénic and Fast modes and represents a challenge to measure them.

Fast modes have isotropic power spectrum and produce the anisotropy solely due to the anisotropy built into F -tensor, Eq. (73), which is somewhat different in the cases of high and low β plasma. Predictions of the quadrupole from the Fast modes are given in the left panel of Figure 10. There are two parameters, β , and the mean deviation of the local field direction $\bar{\chi}$. At each $\bar{\chi}$, for which three are shown, $\cos^{-1} \bar{\chi} = \pi/16, \pi/6, \pi/3$, D_2/D_0 from Fast modes lie distinctly in a narrow band limited by $\beta \gg 1$ and $\beta \ll 1$ predictions according to Eq. (75) and Eq. (74) respectively. The Fast mode quadrupole anisotropy is rather uniform as the function of the orientation angle at $\theta > \pi/6$ and at its maximum is smaller in magnitude than that from Alfvénic modes. Fast mode signal becomes nearly isotropic as field

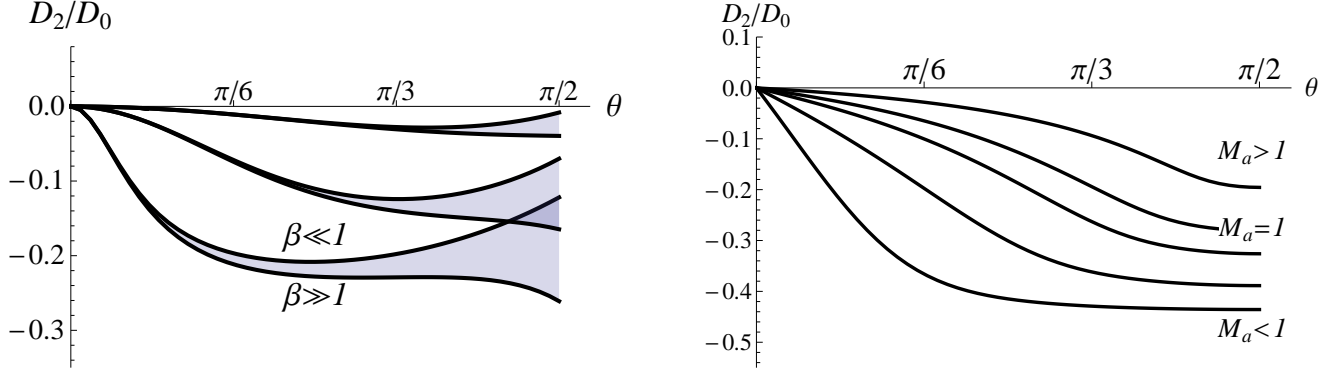


FIG. 10.— Quadrupole of the synchrotron structure function in the units of the monopole versus the mean magnetic field to the line-of-sight angle θ . Left: Fast mode contribution shown in bands for $\cos^{-1} \bar{\chi} = \pi/16, \pi/6, \pi/3$, D_2/D_0 , decreasing in magnitude with increased field wandering. Each band corresponds to the range of different plasma β , bounded by $\beta \gg 1$ and $\beta \ll 1$ limits. Right: the same quantity for the mix of Alfvén and Slow modes in the regime of strong incompressible turbulence. The curves correspond to $M_a = 0.1, 0.4, 0.7, 1, 2$ (from lower to upper ones).

wandering increases, being only at 5% when local wandering is similar to $M_a = 2$ of Alfvénic case. The synchrotron quadrupole from Fast modes is never expected to exceed $|D_2/D_0| \approx 0.25$. Thus, measuring higher quadrupole will put the importance of the Fast modes under question.

As the last exercise we are considering the mix of Alfvén and Slow modes in the regime of strong incompressible turbulence. This is the regime of pure E –type modes with Alfvén like power spectrum distribution and 3D isotropic tensor spectral tensor as modeled in Eq. (79). The results in the right panel of Figure 10 shows that the synchrotron quadrupole structure in this model is very close to that of Alfvénic turbulence. This confirms again that exact local structure of the spectral tensor in Alfvénic turbulence is not decisive in determining the observable quadrupole of the synchrotron. It is primarily reflects the anisotropic distribution of power in the cascade.

6. DISCUSSION

Our paper is aimed to provide the quantitative analytical description of the statistics of synchrotron fluctuations. In this section we discuss what our results mean in terms of observations and what is the relation of this work with previous related publications.

6.1. Our advances in describing synchrotron intensity statistics

Synchrotron fluctuations can be characterized statistically by the slope of their spectrum and their amplitude. In this paper we have obtained expressions for the synchrotron fluctuation amplitude and have shown that the spectral slope of fluctuations depends weakly on the spectral index of relativistic electrons. The latter presents a substantial advance compared to the earlier studies, which were providing expressions for just one electron spectral index, namely, $\gamma = 2$ and were not able to estimate the errors arising from this assumption. Our approximation for correlations at arbitrary γ , namely,

$$D_{sync,\gamma}(\mathbf{R}) \approx \mathcal{A}(\gamma) \sigma^{2\gamma-4} D_{sync,\gamma=2}(\mathbf{R}) \times \frac{(1-\epsilon^2)^\gamma}{1+\epsilon^2} \left[(1-\epsilon^2)^{\frac{1}{2}} \Gamma(1+\gamma) {}_2F_1\left(\frac{1}{2} + \frac{\gamma}{2}, 1 + \frac{\gamma}{2}, 1, \epsilon^2\right) - \Gamma\left(1 + \frac{\gamma}{2}\right)^2 {}_2F_1\left(\frac{1}{2} + \frac{\gamma}{4}, 1 + \frac{\gamma}{4}, 1, \epsilon^2\right)^2 \right] \quad (81)$$

where $\sigma^2 = \sigma_{xx} + \sigma_{yy}$ are magnetic field dispersions and $\epsilon \equiv \frac{\sigma_{xx} - \sigma_{yy}}{\sigma_{xx} + \sigma_{yy}}$ is the degree of anisotropy (see more in §3, Eq. (81)) allows to express the statistics of fluctuations through the statistics obtained for $\gamma = 2$. This expression opens avenues for analysis of the synchrotron intensities for a variety of astrophysical circumstances, for which γ substantially deviates from 2. In other words, synchrotron intensity studies for which possible statistical description was earlier limited to a very special case of a single and unique spectral index of cosmic rays has been extended to a wide range of spectral indexes which encompass astrophysically important situations. Eq. (81) is our first major result.

Earlier studies were limited mostly to hypothetical isotropic magnetic turbulence (see Chepurnov 1998). This would provide a very special and rather unrealistic form for $D_{sync,\gamma=2}$ in Eq. (81). Thus the second part of our paper was devoted to obtaining adequate forms for $D_{sync,\gamma=2}$.

Unlike other earlier studies (see Lazarian & Shutenkov 1990), we avoided dividing magnetic field into the regular and turbulent components. Such a division is unrealistic in view of modern day understanding of turbulence. Instead, in the presence of mean magnetic field, we adopted the model of the axially symmetric magnetic turbulence, where the mean field is directed along the direction of the axis. Both theory and simulations are suggestive that this description should correspond well in the global frame of reference, related to the mean magnetic field (see Lazarian & Vishniac 1999; Cho & Vishniac 2000; Cho et al. 2002). To describe the axially symmetric magnetic turbulence we used the general expressions in Oughton et al. (1997), which generalize the classical results in Batchelor (1946) and Chandrasekhar

(1950). With this, our expression provided a combination of two different tensors with two functions E and F in front of them. At this point one can establish the existence of the anisotropy of synchrotron signal and its relation to the aforementioned functions.

To move one step further, we adopted a model of compressible MHD turbulence from Cho & Lazarian (2002, 2003) and expressed the statistics of the Alfvén, slow and fast modes in terms of the combinations of E and F functions. This allowed us to express the expected anisotropies of the synchrotron emission through the physically motivated basic modes existing in MHD turbulence. Our approach allows to predict the synchrotron emission statistics if the turbulence is defined and, alternatively, study fundamental properties of MHD turbulence analyzing spectra and anisotropies of the synchrotron statistics.

While we believe that the decomposition into modes in Cho & Lazarian (2002, 2003) is well motivated theoretically and proven numerically, our approach in the present paper can be applied to any arbitrary model of axisymmetric turbulence. For instance, it can be applied to test the predictions of the model of MHD turbulence consisting from slab and 2D fluctuations⁹ (Matthaeus et al. 1990; Zank & Matthaeus 1993). We are far from assuming that astrophysical magnetized compressible turbulence is completely understood. For instance, recent numerical simulations in Federrath et al. (2008, 2009, 2010) demonstrate the effects of turbulence injection on the resulting turbulence. In the presence of multiple sources of energy injection, instabilities and damping processes the spectrum of magnetic turbulence inferred from synchrotron observations may be rather complex. Our description accounts for turbulence compressibility and our analytical expressions can be used for turbulence with several injection scales. This opens avenues for realistic magnetic turbulence in its complexity.

6.2. Studying magnetic field direction

Our results show that magnetic field direction can be studied through the analysis of the anisotropy of synchrotron intensity correlation functions. This provides a synergetic way of studying magnetic fields.

Other approaches to studying magnetic field direction are known in the literature. Some of them are based on direct measurements of synchrotron polarization (see Ginzburg 1981), polarization from aligned grains (see review by Lazarian 2007 and references therein), or aligned atoms (see Yan & Lazarian 2008). In addition, a statistical determination of the mean magnetic field direction is possible with the statistical analysis of the Doppler shifted lines (Lazarian et al 2002; Esquivel & Lazarian 2005, 2011), that has similarities with the one we proposed here. In this technique the difference in velocity correlations parallel and perpendicular to mean magnetic field also reveals the direction of magnetic field. The aforementioned difference was recently used to find the direction of magnetic field in interstellar gas (Heyer et al. 2008).

All these techniques measure magnetic field in different media and have their limitations. For instance, the technique based on the analysis of spectral lines is not applicable to hot rarefied halo gas with little emission. Studying aligned dust in the latter environment is also extremely challenging. At the same time, this is the domain of the new technique. Needless to say that obtaining the same direction of the magnetic field with different techniques increases the confidence of the result, while the discrepancy in the directions may testify on the existence of different regions with different conditions and different direction of magnetic field along the line of sight.

6.3. Towards a cookbook for synchrotron studies

Turbulence in our galaxy is believed to span from hundreds of parsec to hundreds of kilometers. This follows both from the analysis of electron density fluctuations (Armstrong et al. 1994, Chepurnov & Lazarian 2010), spectral lines (Larson 1981, see Lazarian 2009 and ref. therein), synchrotron fluctuations (see Cho & Lazarian 2010 and ref. therein) etc. With synchrotron emission one expects to measure fluctuations arising from magnetic fluctuations starting from the largest scale to very small scales, where the physical limitations on the small scale arise either from turbulence damping or Larmor radius of relativistic electrons. The practical limitations on turbulence studies will arise from both noise and the resolution of the data. As turbulence fluctuations decrease in amplitude corresponding to the Kolmogorov power spectrum, i.e. with the two dimensional measured spectrum $P_2 \sim K^{-11/3}$, the small scale fluctuations are more subjected to the effect of noise.

The new generation of telescopes (e.g. SKA, LOFAR) present observers with lower noise and higher resolution data which should enable them to reliably study synchrotron fluctuations over a wider range of scales. This will open prospects of detailed studies magnetic turbulence not only in Milky Way but also in supernovae remnants, radio lobes and external galaxies. For this wide variety of objects electron spectral index varies, but our present work shows that this is not a problem.

Our present paper opens a new dimension in studies of synchrotron maps. Apart from getting the spectral index of magnetic turbulence, our analytical results testify that by the analysis of synchrotron anisotropies one can obtain the direction of magnetic field. Moreover, it can also deliver very unique piece of information, i.e. the relative contribution of compressible versus incompressible motions. Indeed, our study of the spatial multipoles of the synchrotron correlations shows that the signatures of Alfvénic and fast-wave turbulence are different. These signatures can be studied observationally to identify regions with different degrees of compressibility. Does higher or lower compressions of magnetic field correlate to higher star formation rate? What about compressibility and magnetic field amplification?

⁹ We believe that this model may represent only transient state of the actual MHD turbulence and is not physically motivated in terms of cascades of turbulent energy.

These can be the questions that one will be able to answer analyzing synchrotron maps and correlating the results with other astrophysical data.

6.4. *Statistics of synchrotron polarization*

While most of the present paper is devoted to studies of intensities, in Appendix E we provide the description of the fluctuations of other Stocks parameters and their combination. This provides an important extension of the approach suggested in this paper.

We noticed that the structure of the correlations of other Stocks parameters is similar to that of intensity. On the basis of this we could conjecture that the dependence of the correlations involving polarization will be similar to the correlations of intensity, i.e. with the dependence on the cosmic ray spectral index affecting mostly the prefactor of obtained correlations. Numerical studies of synchrotron fluctuations with cosmic rays corresponding to different γ in Ensslin et al. (2010) are suggestive of this outcome.

In any case, in Appendix E, in analogy with the rest of the paper, we provided calculations of correlations of other Stocks parameters and their combinations. We observe that that combining intensity and polarization statistics one can remove the degeneracies, for instance, arising from the unknown 3D direction of the mean magnetic field, which determines the axis of anisotropy for magnetic turbulence. The bonus of combining the statistics of polarization and intensity could be determining of this 3D direction. This study should be continued.

Our study opens avenues of addressing subtle issues related to magnetic field structure. For instance, Waelkens et al. (2009) proposed to study tension force spectrum from fourth order statistics of polarized data. They, however, used the isotropic model of turbulence, which does not correspond to what we now know about magnetic turbulence. Our approach allows such studies within a realistic model of magnetic turbulence.

In Appendix E we gave, for completeness, the expressions for the sky-projected structure functions between the line-of-sight components of the magnetic field. While not appearing in synchrotron intensity studies, the line-of-sight part of the magnetic field is important in describing the Faraday rotation of the polarization direction.

Having the statistical description of synchrotron fluctuations and the effects of Faraday rotation on the fluctuations we open prospects of describing the statistics of synchrotron polarization data cubes which contain synchrotron polarization map for different frequencies (see Haverkorn 2010, Gaensler et al. 2011). Our approach opens ways to provide detailed quantitative description of such data cubes.

6.5. *Synchrotron foreground for CMB and high-redshift HI studies*

It is important to stress, that the description that we obtained is important for both studying galactic and extragalactic magnetic fields and for removing the synchrotron fluctuations from cosmological CMB fluctuations as well as from the fluctuations high redshifted atomic hydrogen which can provide a unique insight into the processes at the beginning of the Universe.

We expect our description to be important for studies of galactic synchrotron foregrounds. In terms of weeding out the foreground fluctuations, a procedure of partial filtering was developed in Cho & Lazarian (2010). It was proven there that the galactic foreground fluctuations, e.g. synchrotron fluctuations, arise from galactic turbulence with the spectral index of fluctuations that depends on the spectral index of the underlying turbulence and the geometry of the emitting turbulent volume. This determinism allows one to predict the fluctuations of foreground emission at a given scale, provided that the foreground fluctuations are measured at a different scale. The procedure is applicable to both spatial filtering of CMB signal and high redshifted HI emission from the early Universe. For instance, if synchrotron is separated in low resolution measurements, the procedure in Cho & Lazarian (2010) allows to remove its contribution for high resolution measurements. The accuracy of the removal increases if we know more about the expected power law of the spatial fluctuations. In view of this the effect of γ not being equal to the value 2 assumed in the estimates was a concern. Our present work removes this concern and allows to use the procedure in Cho & Lazarian (2010) with higher confidence.

Our obtaining in Appendix E of the tensor of synchrotron polarization should also help to weeding off the polarized galactic synchrotron foreground. This foreground is known to be important for the CMB polarization studies, in particular, for the studies of the illusive B-modes.

In general, the more we know about the synchrotron statistics, the more reliable is its removal. For instance, if the filtered signal show the anisotropies expected from the synchrotron emission, this would testify that the synchrotron foreground was not properly removed. Additional, more sophisticated procedures may also be developed. For instance, the procedure of foreground removal proposed in Cho & Lazarian (2010) requires the best possible knowledge of the foreground spectrum at one spatial resolution in order to remove the foreground at another resolution. The a priori knowledge of what we expect in terms of the anisotropy of the synchrotron statistics help to determine the foreground statistics with higher accuracy.

6.6. *Anisotropic part of synchrotron correlation tensor*

In this paper we provided a detailed analysis of the expected properties of the anisotropies of synchrotron fluctuations. These anisotropies were also of interest for earlier studies, which were strongly limited in applicability because both of the assumption about the assumed single value of electron spectral index and of the assumed models of magnetic turbulence. These earlier studies are of interest as the approach presented in our paper allows to cure their deficiencies.

For instance, a technique for obtaining the size of galactic halo was proposed in Lazarian & Chibisov (1991). The authors proposed to use HII regions as distance indicators and calculate anisotropic part of synchrotron intensity

correlations for the directions towards and away from the HII region. Choosing sufficiently long radio wavelengths for which HII regions are opaque, one can probe magnetic fields on the scale of the distance from the observer to the HII region. These correlation functions were to be compared with the correlation functions obtained for both lines of sight avoiding HII region or with correlation functions at the wavelengths for which the HII regions are transparent.

It is possible to see that if the angular scale of synchrotron fluctuations is θ and the distance to the HII region is D , the physical size of the magnetic fluctuations is $\sim D \sin \theta$. If the angular scale of synchrotron fluctuations is θ' , then the ratio of the halo size to the size of the distance to the HII region will be $\sin \theta / \sin \theta'$. Our study of the weak dependence of synchrotron statistics expressions on γ gives more confidence that similar studies using anisotropic part of the correlation tensor can be done in practice.

6.7. Effects of cosmic rays

The fact that the expression for synchrotron intensity depends on the spectral index of cosmic rays has been an impediment for the quantitative studies of the statistics of synchrotron variations. Our study shows that cosmic ray spectral variations change only the amplitude of the synchrotron variations and do not change the angular dependences of the correlation and structure functions of the synchrotron intensities (see Eq. (81)). They do not change the direction of the anisotropies either. This simplifies the interpretation of the observations.

Our study has been performed in the assumption of no magnetic field correlation with the density of relativistic electrons. This assumption corresponds to observation of much smoother distribution of relativistic electrons compared to the distribution of magnetic fields in the Milky Way. Our formalism, however, may be extended for the case of relativistic electrons correlated with magnetic fields. We do not expect substantial changes in our present conclusions, e.g. in the dependence of synchrotron intensity spectrum on γ .

6.8. Complex geometry of observations

In the paper we assumed that synchrotron emission is coming to the observer from a single region. Even in this case, the statistics of fluctuations can change from geometrical effects of observing galactic turbulence. For angles ϕ between lines of sight less than L_{turb}/D_{obj} where L_{turb} is the turbulence injection scale and D_{obj} is the size the observed region size along the line of sight, the spectral index of the angular spectrum of synchrotron fluctuations coincides with the spectral index of synchrotron emissivity fluctuations. For larger angles the spectral index changes. In an idealized case of uniform turbulence surrounding an observer, it gets universal corresponding to the correlation function of intensity $\sim \phi^{-1}$. This effect was first discussed in Shutenkov & Lazarian (1990) and attributed to the converging lines of sight geometry of observations. Later the change of the spectral index of synchrotron fluctuations was confirmed with the analysis of the observational data¹⁰ in Cho & Lazarian (2002). This paper reveals the relation of the spectral index of synchrotron emissivity with the spectral index of underlying magnetic turbulence which shows that for $\phi < \phi_{max} = D_{obj}/L$ we get the actual spectrum of the underlying magnetic turbulence.

For studies of synchrotron emission in a volume that does not surround the observer, as this is the case for extragalactic studies, it is possible to show that the direct relation of the spectral index of angular fluctuations and the underlying magnetic turbulence is preserved if $\phi < \theta_{max} = \Delta_{obj}/L$, where Δ_{obj} is the extend of the emitting volume along the line of sight. This is the regime that one is mostly interested in.

In terms of anisotropy studies, both regimes of $\phi > \phi_{max}$ and $\phi < \phi_{max}$ allow determination of the magnetic field direction. This is true for both galactic and extragalactic studies.

If the observations are done looking through multiple disconnected turbulent volumes with uncorrelated direction of magnetic field, a decrease of the degree of anisotropy is expected. Naturally, this is not the best case for studies of turbulence either. Provided that for all regions along the line of sight ϕ is less than ϕ_{max} , one is expected to obtain the same power spectral index provided that for all volumes we study, synchrotron fluctuations arise from turbulence in the inertial range.

6.9. Synergy of techniques for studying turbulence spectra

In the section above we have discussed the advantages of using synchrotron fluctuations for studies of the ISM. However, the technique of magnetic turbulence study that we propose in the present paper should be viewed as a technique complementary to other existing techniques. We believe that the most interesting questions can be answered if properties of turbulence in different parts of the galaxy and in different ISM phases are compared.

In addition to the magnetic field turbulence spectrum discussed in our paper it is advantageous to study also spectra of density and velocity. If the study of the former is rather straightforward from the column density maps (see Stutzki 1999), studying velocity is far from trivial. In fact, our studies in Esquivel & Lazarian (2005); Esquivel et al. (2007) revealed that a routinely adopted tool for turbulent velocity studies, namely, velocity centroids¹¹ cannot reliably reveal velocity fluctuations for supersonic turbulence. However, two new techniques termed Velocity Channel Analysis (VCA) and Velocity Coordinate Spectrum (VCS) have been introduced during the last decade (Lazarian & Pogosyan 2000, 2004, 2006, 2008). These techniques have been successfully tested and applied to observational data (Lazarian et al.

¹⁰ It is worth mentioning that the change of the spectral index reported in Cho & Lazarian (2002) on the basis of the analysis of data sets for high latitude synchrotron emission as well as for synchrotron emission from the disk is consistent with the injection scale of 100 pc.

¹¹ One may also use so-called "modified velocity centroids" (Lazarian & Esquivel 2003), but those, while increasing the range of applicability of centroids and increasing their accuracy in tracing velocities, still cannot be applied for the observational studies of high Mach number turbulence.

2001; Padoan et al. 2006, 2009; Chepurnov & Lazarian 2009; Chepurnov et al. 2010, see also review in Lazarian (2009) for the references therein). They allow to reliably retrieve data on velocity spectra from the Doppler shifted emission and absorptions lines.

We would like to stress that the overall shape of the turbulence spectrum and its spectral index can be very informative. The former provides information about the sources and sinks of turbulence, the latter characterizing the cascading of energy and, possibly, the role of plasma instabilities acting in collisionless media. Thus advantages and insight arising from the ability of obtaining of magnetic field spectra and comparing its to spectra obtained in Doppler shifted lines are difficult to overestimate.

Spectrum is not the only measure of turbulence. New techniques to study sonic and Alfvénic Mach numbers (i.e. M_s and M_A , respectively) of turbulence have been developed recently. They include so called Tsallis statistics (see Burlaga & F. Viñas 2004a,b, 2005, 2006; Burlaga et al. 2006a,b, 2007, 2009; Esquivel & Lazarian 2010; Tofflemire et al. 2011), bi-spectrum (see Burkhart et al. 2009, 2010), genus analysis (see Chepurnov et al. 2008), etc. They allow us to get a comprehensive picture of magnetic turbulence. Our analysis also provides a synergetic way of studying magnetic field compressibility. For instance, synchrotron fluctuations may map extended turbulent volume of the galactic halo. The relation of this turbulence taking place in tenuous plasma to the turbulence of atomic and molecular species which can be revealed with the VCA and VCS techniques. This will be very valuable for understanding of the complex interrelated dynamics of ionized and neutral media in our galaxy.

In addition, the detailed work that we performed in this paper on describing of anisotropy of synchrotron fluctuations arising from anisotropic magnetic turbulence will benefit other directions of turbulence studies. Similar anisotropies arise, for instance in velocity fluctuations. These anisotropies were suggested by Lazarian, Pogosyan & Esquivel (2002) as a means of studying the magnetic field direction and were shown to be present both in channel maps of position-position-velocity (PPV) data cubes of synthetic data and in the statistics obtained with velocity centroids. Later, velocity centroids were studied in Esquivel & Lazarian (2005, 2011) with synthetic data corresponding to numerical simulations with different Mach numbers, M_s and M_A , and empirical dependences of the degree of anisotropy on these numbers was obtained. Applying the analytical approach developed in this paper it is possible to separate contributions of the compressible and Alfvénic parts of the magnetic turbulence similar as we described above. This is going to provide new ways of detailed quantitative studies of interstellar turbulence using the wealth of spectroscopic surveys.

7. SUMMARY

Our study has revealed the following important properties of the statistics of synchrotron fluctuations:

1. In terms of functional dependence, the spectrum of spatial synchrotron fluctuations marginally depends on the spectral index of relativistic electrons, while the amplitude of the fluctuations depends on the relativistic electron spectral index.
2. Magnetic turbulence makes fluctuations of synchrotron radiation anisotropic with the direction anisotropy given by the averaged mean magnetic field. As we found that the quadrupole anisotropy is the most prominent, this provides a new way of studying the direction of magnetic field using just synchrotron intensity variations.
3. The relation between the isotropic and anisotropic parts of the synchrotron intensity fluctuations provides a way to study the compressibility of magnetic turbulence.

AL acknowledges the NSF grant AST 0808118, NASA grant NNX11AD32G and the support of the Center of Magnetic Self-Organization (CMSO). Humboldt Award and related stimulating stay in Universities of Cologne and Bochum is also acknowledged by AL. AL and DP thank Mark Baker for many useful discussions and reviewing the formulas in Appendix B.

APPENDIX

A. TABLE OF NOTATION

B. AXISYMMETRIC STATISTICS OF VECTOR FIELDS

B.1. From power spectrum to correlation function

Let us consider axisymmetric MHD turbulence that is described by a single power E – type power spectrum

$$E(\mathbf{k}) = E(k, \mathbf{k} \cdot \hat{\lambda}) \left(\delta_{ij} - \hat{k}_i \hat{k}_j \right) \quad (\text{B1})$$

This is not the most general case of axisymmetric spectrum, since in general one can have four independent spectral functions. However, this ansatz arise in the regime of strong incompressible MHD turbulence where contribution of Alfvénic and slow modes is similar, as found in numerical simulations by Cho & Lazarian (2003).

Let us consider what structure functions correspond to these models. We start from the general expression for the correlation function

$$\langle H_i(\mathbf{x}_1) H_j(\mathbf{x}_2) \rangle = \int d^3 \mathbf{k} e^{i \mathbf{k} \cdot \mathbf{x}} E(\mathbf{k}) \left(\delta_{ij} - \hat{k}_i \hat{k}_j \right) \quad (\text{B2})$$

TABLE A1
LIST OF NOTATIONS

$\hat{\lambda}$	unit vector of direction of the statistical symmetry axis (mean magnetic field)
z-axis	is along the line of sight
y-axis	is perpendicular to both the line of sight and the symmetry axis $\hat{\lambda}$
x-axis	is perpendicular to the line of sight and parallel to the sky projection of the symmetry axis $\hat{\Lambda}$
$\mathbf{x}_1, \mathbf{x}_2 \dots$	3D position vectors
\mathbf{r}, r	3D separation vector and its magnitude, $\mathbf{r} = (\mathbf{R}, z)$
$\mathbf{k}, k, \hat{\mathbf{k}}$	3D wave vector and its magnitude, $\mathbf{k} = (\mathbf{K}, k_z)$, and the unit vector $\hat{\mathbf{k}} = \mathbf{k}/k$
μ	cosine of the angle between the 3D wave vector and the symmetry axis $\mu = \hat{\mathbf{k}} \cdot \hat{\lambda}$
$\hat{\Lambda}$	2D unit vector of the sky projection of the symmetry axis $\hat{\lambda}$
$\mathbf{X}_1, \mathbf{X}_2 \dots$	2D position vectors
\mathbf{R}, R	2D sky projection of the separation vector and its magnitude
$\mathbf{K}, K, \hat{\mathbf{K}}$	2D wave vector and its magnitude, and the unit vector $\hat{\mathbf{K}} = \mathbf{K}/K$
ψ	polar angle between 2D wave vector \mathbf{K} and the x-axis, $\hat{\mathbf{K}} = (\cos \psi, \sin \psi)$
ϕ	polar angle between 2D separation \mathbf{R} and the x-axis
$I_{sync}(\mathbf{X})$	intensity of synchrotron emission
$\xi_{sync}(\mathbf{R}), D_{sync}(\mathbf{R})$	correlation/structure function of synchrotron intensity
$\tilde{\xi}_{sync}(\mathbf{R}), \tilde{D}_{sync}(\mathbf{R})$	normalized correlation/structure function of synchrotron intensity
$\tilde{D}_n(\mathbf{R})$	coefficient of the multipole decomposition of $\tilde{D}_{sync}(\mathbf{R})$
$H_{\perp}(\mathbf{x})$	magnitude of the component of the magnetic field orthogonal to the line of sight.
$\xi_{H_{\perp}}(\mathbf{r}), D_{H_{\perp}}(\mathbf{r})$	3D correlation/structure function of γ 's power of $H_{\perp}(\mathbf{r})$
$\tilde{\xi}_{H_{\perp}}(\mathbf{r}), \tilde{D}_{H_{\perp}}(\mathbf{r})$	normalized 3D correlation/structure function of γ 's power of $H_{\perp}(\mathbf{r})$
$E(\mathbf{k}), F(\mathbf{k})$	3D power spectra functions. For axisymmetric turbulence $E(\mathbf{k}) = E(k, \mu)$ and $F(\mathbf{k}) = F(k, \mu)$
E_l, F_l	multipole coefficient of Legendre expansion of $E(k, \mu)$ and $F(k, \mu)$ in μ
$\hat{E}(\mu), \hat{F}(\mu)$	angular dependence of $E(k, \mu)$ and $F(k, \mu)$ if scale dependence is factorized
\hat{E}_l, \hat{F}_l	multipole coefficient of Legendre expansion of $\hat{E}(\mu)$ and $\hat{F}(\mu)$
$\sigma_{ }, \sigma_{\perp}$	variances of the magnetic field components parallel and perpendicular to the symmetry axis (mean field)
r_{σ}	ratio of $\sigma_{ }$ and $1/2\sigma_{\perp}$
$E(\mathbf{K}), F(\mathbf{K})$	$E(\mathbf{k}), F(\mathbf{k})$ with $k_z = 0$, power spectra of the fluctuations integrated along the line of sight
$E_n, F_n, \hat{E}_n, \hat{F}_n$	coefficients of the harmonic expansion of $E(\mathbf{K})$ and $F(\mathbf{K})$ or their factorized version
σ_{xx}, σ_{yy}	variances of the x and y magnetic field components
ϵ	anisotropy measure of the variance of the sky components of the magnetic field, $\epsilon = \frac{\sigma_{xx} - \sigma_{yy}}{\sigma_{xx} + \sigma_{yy}}$
D_{ij}, D_{zz}	2D sky and line-of-sight components of the z-integrated correlation (structure) tensor of the magnetic field
D^+, D^-, D^{\times}	$D^+ = D_{xx} + D_{yy}$, $D^- = D_{xx} - D_{yy}$, $D^{\times} = D_{xy}$
$\hat{\lambda}_0$	unit vector of direction of the global symmetry axis in case of mean field wandering
$\bar{\chi}$	average cosine of the angle between the local and the global symmetry directions
$W_I(\bar{\chi})$	weight of the isotropized spectral part
$W_L(\bar{\chi})$	weight of the local anisotropic spectral part
$G^A(\psi, \theta), G^F(\theta)$	geometric functions describing the 2D structure of the turbulent mode
$G_n^A(\theta), G_n^F(\theta)$	multipole decomposition of the geometric functions
r_I	energy injection scale
β	plasma constant
M_a	Alfvénic Mach number

and rewrite it as

$$\begin{aligned}
\langle H_i(\mathbf{x}_1) H_j(\mathbf{x}_2) \rangle &= \left[\frac{\partial}{\partial r_i} \frac{\partial}{\partial r_j} - \delta_{ij} \Delta \right] \int dk d\Omega_{\mathbf{k}} e^{i\mathbf{k} \cdot \mathbf{x}} E(k, \mathbf{k} \cdot \hat{\lambda}) \\
&= \left[\frac{\partial}{\partial r_i} \frac{\partial}{\partial r_j} - \delta_{ij} \Delta \right] \Phi(r, r\mu)
\end{aligned} \tag{B3}$$

Scalar function $\Phi(r, r\mu)$ depend on r and $\alpha = \mathbf{r} \cdot \hat{\lambda} = r\mu$. Following Chandrasekhar (1950), it is convenient to introduce the following differential operators

$$D_r = \frac{1}{r} \frac{\partial}{\partial r} \Big|_{\alpha=const} = \frac{1}{r} \frac{\partial}{\partial r} - \frac{\mu}{r} \frac{\partial}{\partial \mu}, \quad D_{\mu} = \frac{\partial}{\partial \alpha} \Big|_{r=const} = \frac{1}{r} \frac{\partial}{\partial \mu} \tag{B4}$$

Notice, that D_r reflects partial derivative with respect to r when α , rather than μ is kept constant. D_{μ} is actually derivative with respect to α and has dimensions of $1/r$.

In terms of these differential operators, the tensor of second partial derivatives and the Laplacian of an axisymmetric function are

$$\frac{\partial^2}{\partial r_i \partial r_j} \Phi(r, r\mu) = r_i r_j D_{rr} \Phi + \delta_{ij} D_r \Phi + \hat{\lambda}_i \hat{\lambda}_j D_{\mu\mu} \Phi + (r_i \hat{\lambda}_j + r_j \hat{\lambda}_i) D_{r\mu} \Phi \quad (\text{B5})$$

$$\Delta \Phi(r, r\mu) = (r^2 D_{rr} + 3D_r + D_{\mu\mu} + 2r\mu D_r D_\mu) \Phi \quad (\text{B6})$$

and one obtains

$$\langle H_i(\mathbf{x}_1) H_j(\mathbf{x}_2) \rangle = (r^2 D_{rr} \Phi) \hat{r}_i \hat{r}_j + (D_r - \Delta) \Phi \delta_{ij} + D_{\mu\mu} \Phi \hat{\lambda}_i \hat{\lambda}_j + r D_{r\mu} \Phi (\hat{r}_i \hat{\lambda}_j + \hat{r}_j \hat{\lambda}_i) \quad (\text{B7})$$

that leads to the following identification of the correlation coefficients

$$A_\xi = r^2 D_{rr} \Phi, \quad B_\xi = (D_r - \Delta) \Phi, \quad C_\xi = D_{\mu\mu} \Phi, \quad D_\xi = r D_{r\mu} \Phi. \quad (\text{B8})$$

B.2. Multipole decomposition

Decomposition of the plain wave and the spectrum in spherical harmonics

$$e^{i\mathbf{k} \cdot \mathbf{x}} = 4\pi \sum_l i^l j_l(kr) \sum_{m=-l}^l Y_{lm}(\hat{k}) Y_{lm}^*(\hat{r}) \quad (\text{B9})$$

$$E(k, \mathbf{k} \cdot \hat{\lambda}) = \sum_{lm} \frac{4\pi}{2l+1} E_l(k) Y_{lm}^*(\hat{k}) Y_{lm}(\hat{r}) \quad (\text{B10})$$

gives after integration over angles $d\Omega_{\mathbf{k}}$

$$\Phi(r, r\mu) = 4\pi \sum_l i^l P_l(\mu) \int dk j_l(kr) E_l(k). \quad (\text{B11})$$

The multiple expansion of the correlation tensor coefficients follows

$$A_\xi = 4\pi \sum_{n=0}^{\infty} i^n P_n(\hat{\mathbf{r}} \cdot \hat{\lambda}) \left[-\tilde{\Upsilon}_n + (3+2n)\tilde{\Gamma}_n - 2(1+2n)\tilde{\Gamma}_{n+2} + (1+2n)(3+2n)\Lambda_{n+4} \right] \\ + 2\pi \sum_{n=0}^{\infty} P_n(\hat{\mathbf{r}} \cdot \hat{\lambda}) (1+2n) \sum_{l=n+4,2}^{\infty} i^l \left[4\tilde{\Gamma}_l - (l(l+1) - n(n+1))\Lambda_{l+2} \right] \quad (\text{B12})$$

$$B_\xi = 4\pi \sum_{n=0}^{\infty} i^n P_n(\hat{\mathbf{r}} \cdot \hat{\lambda}) \left[\tilde{\Upsilon}_n - \tilde{\Gamma}_n + (2n+1)\Lambda_{n+2} \right] \\ - 4\pi \sum_{n=0}^{\infty} P_n(\hat{\mathbf{r}} \cdot \hat{\lambda}) (1+2n) \sum_{l=n+4,2}^{\infty} i^l \Lambda_l \quad (\text{B13})$$

$$C_\xi = 2\pi \sum_{n=0}^{\infty} (1+2n) P_n(\hat{\mathbf{r}} \cdot \hat{\lambda}) \sum_{l=n+2,2}^{\infty} i^l (l-n)(l+n+1) \Lambda_l \quad (\text{B14})$$

$$D_\xi = -2\pi \sum_{n=0}^{\infty} (1+2n) P_n(\hat{\mathbf{r}} \cdot \hat{\lambda}) \sum_{l=n+1,2}^{\infty} i^l \left[2\tilde{\Gamma}_l - ((l+1)(l+2) - n(n+1))\Lambda_{l+2} \right] \quad (\text{B15})$$

where $\tilde{\Upsilon}_l(r) = \int k^2 dk j_l(kr) E_l(k)$, $\tilde{\Gamma}_l(r) = \int k^2 dk \frac{j_{l+1}(kr)}{kr} E_l(k)$ and $\Lambda_l(r) = \int k^2 dk \frac{j_l(kr)}{(kr)^2} E_l(k)$

It is instructive to write out explicitly low multipole terms wrt the angle with the symmetry axis and investigate their behaviour as $r \rightarrow 0$. Leaving only the $r \rightarrow 0$ leading terms, for the monopole

$$A_0(r) \sim 4\pi \int k^2 dk \left[- \left(j_0(kr) - 3 \frac{j_1(kr)}{kr} \right) E_0 - 2 \frac{j_3(kr)}{kr} E_2 + 3 \frac{j_4(kr)}{(kr)^2} E_4 \right] \quad (\text{B16})$$

$$B_0(r) \sim 4\pi \int k^2 dk \left[\left(j_0(kr) - \frac{j_1(kr)}{kr} \right) E_0 + \frac{j_2(kr)}{(kr)^2} E_2 \right] \quad (\text{B17})$$

$$C_0(r) \sim -12\pi \int k^2 dk \left[\frac{j_2(kr)}{(kr)^2} E_2 \right], \quad (\text{B18})$$

and for the next order

$$A_2 \sim 4\pi \int k^2 dk \left[\left(j_2(kr) - 7 \frac{j_3(kr)}{kr} \right) E_2 + 10 \frac{j_5(kr)}{kr} E_4 - 35 \frac{j_6(kr)}{(kr)^2} E_6 \right] \quad (\text{B19})$$

$$B_2 \sim -4\pi \int k^2 dk \left[\left(j_2(kr) - \frac{j_3(kr)}{kr} \right) E_2 + 5 \frac{j_4(kr)}{(kr)^2} E_4 \right] \quad (B20)$$

$$C_2 \sim 140\pi \int k^2 dk \left[\frac{j_4(kr)}{(kr)^2} E_4 \right] \quad (B21)$$

$$D_1 \sim 12\pi \int k^2 dk \left[\frac{j_3(kr)}{kr} E_2 - 5 \frac{j_4(kr)}{(kr)^2} E_4 \right] \quad (B22)$$

At zero separation $r \rightarrow 0$, $A_0(0)$ and $D_0(0)$ while $B_0(0) = 4\pi \int k^2 dk \left[\frac{2}{3} E_0 + \frac{1}{15} E_2 \right]$ and $C_0(0) = -\frac{4\pi}{5} \int k^2 dk E_2$ describe the variance and same-point correlation of the components of the vector field

$$\langle H_i(\mathbf{x}_1) H_j(\mathbf{x}_1) \rangle = B(0) \delta_{ij} + C(0) \lambda_i \lambda_j \quad (B23)$$

Hence, for axisymmetric field not only the variances of the components differ, but there is zero separation correlation between different components if no frame axis is aligned with the symmetry axis.

In case of structure functions one computes $B(0) - B(r), \dots$, which leads to regularization of the monopole terms B_0 and C_0 .

B.3. Derivation of the multipole decomposition

Derivations of the expressions Eqs. (B12-B15) involves evaluating derivatives of the $j_l(kr)P_l(\mu)$ basis functions and rearranging the series in multipole “l”. We start with the following relations for the the angular derivatives

$$\mu \frac{\partial}{\partial \mu} P_l(\mu) = l P_l(\mu) + \sum_{n=(0,1),2}^{l-2} (2n+1) P_n(\mu) \quad (B24)$$

$$\left(\mu \frac{\partial}{\partial \mu} \right)^2 P_l(\mu) = l^2 P_l(\mu) + \frac{1}{2} \sum_{n=(0,1),2}^{l-2} [(l+2)(l-1) - n(n+1)] (2n+1) P_n(\mu) \quad (B25)$$

$$\frac{\partial^2}{\partial \mu^2} P_l(\mu) = \frac{1}{2} \sum_{n=(0,1),2}^{l-2} (l-n)(l+n+1)(2n+1) P_n(\mu) \quad (B26)$$

where the notation $\sum_{n=(0,1),2}$ means that the sum over n starts from the first value in the parenthesis (zero) when l is even and from the second one (unity) when l is odd, and proceeds with the step of two. The sums are zero for $l = 0, 1$.

For the radial derivative we shall use

$$\frac{1}{k} \frac{\partial}{\partial r} j_l(kr) = \frac{l}{kr} j_l(kr) - j_{l+1}(kr) \quad (B27)$$

Now we can write out the actions of several operators that we need. The following expressions show some intermediate steps, and for the final conclusion point to the structure that the operator creates in the full multipole expansion after the integration over k has been carried out

$$\begin{aligned} D_r [j_l(kr) P_l(\mu)] &= P_l(\mu) \frac{1}{r} \frac{\partial}{\partial r} j_l(kr) - \frac{j_l(kr)}{r^2} \mu \frac{\partial}{\partial \mu} P_l(\mu) = -k^2 \frac{j_{l+1}(kr)}{kr} P_l(\mu) - k^2 \frac{j_l(kr)}{k^2 r^2} \sum_{n=(0,1),2}^{l-2} (2n+1) P_n(\mu) \\ &\rightarrow -\tilde{\Gamma}_l(r) P_l(\mu) - \Lambda_l(r) \sum_{n=(0,1),2}^{l-2} (2n+1) P_n(\mu) \quad , \end{aligned} \quad (B28)$$

$$r \mu D_\mu D_r [j_l(kr) P_l(\mu)] = \left(\mu \frac{\partial}{\partial \mu} \right) D_r [j_l(kr) P_l(\mu)] \quad (B29)$$

$$\rightarrow -\tilde{\Gamma}_l(r) \left[l P_l(\mu) + \sum_{n=(0,1),2}^{l-2} (2n+1) P_n(\mu) \right] - \frac{1}{2} \Lambda_l(r) \sum_{n=(0,1),2}^{l-2} [(l+1)(l-2) - n(n+1)] (2n+1) P_n(\mu)$$

$$D_{\mu\mu} [j_l(kr) P_l(\mu)] = k^2 \frac{j_l(kr)}{k^2 r^2} \frac{\partial^2}{\partial \mu^2} P_l(\mu) \rightarrow \frac{1}{2} \Lambda_l(r) \sum_{n=(0,1),2}^{l-2} (l-n)(l+n+1)(2n+1) P_n(\mu) \quad , \quad (B30)$$

$$\Delta (j_l(kr) P_l(\mu)) = -k^2 j_l(kr) P_l(\mu) \rightarrow -\tilde{\Upsilon}_l(r) P_l(\mu) \quad (B31)$$

Multipole expansion of the correlation coefficients now follows from combination of the above results. In order to obtain the final expressions, we make two important steps. Firstly we change the order of summation $\sum_{l=0}^{\infty} \sum_{n=(0,1),2}^{l-2} = \sum_{n=0}^{\infty} \sum_{l=n+2,2}^{\infty}$ and take the label for the exterior sum to be n everywhere. Secondly we collect together the lowest order terms of the same power of divergence in k integrals.

Let us proceed in the order of difficulty

B.3.1. C_ξ

C_ξ is obtained directly from Eq. (B30).

B.3.2. B_ξ

B_ξ is a combination of Eq. (B28) and Eq. (B31). Let us illustrate the reversal of the summation order on this example. Using n for the exterior index the direct combination of two equations and the change of the summation order in the double sum gives

$$B_\xi = 4\pi \sum_{n=0}^{\infty} i^n P_n(\mu) \left(\tilde{\Upsilon}_n - \tilde{\Gamma}_n \right) - 4\pi \sum_{n=0}^{\infty} (2n+1) P_n(\mu) \sum_{l=n+2,2}^{\infty} i^l \Lambda_l \quad (\text{B32})$$

It is important that Λ_0 contribution is not present since the integral in $\Lambda_n \propto j_n(kr)/(kr)^2 \sim (kr)^{n-2}$ is potentially the most divergent one. $\tilde{\Upsilon}_n \sim j_n(kr) \sim (kr)^n$ and $\tilde{\Gamma}_n \sim j_{n+1}(kr) \sim (kr)^n$ has the same level of potential divergence as Λ_{n+2} . These considerations are important for the steep spectra that play role in turbulence studies, where correlation functions are not formally determined at long wavelengths, and transition to regularized structure function must be performed. Such transition amounts to regularization of the integrals, mainly in Λ_n . Thus, we group the $l = n+2$ term from the double sum together with the first term to get

$$B_\xi = 4\pi \sum_{n=0}^{\infty} i^n P_n(\mu) \left(\tilde{\Upsilon}_n - \tilde{\Gamma}_n + (2n+1)\Lambda_{n+2} \right) - 4\pi \sum_{n=0}^{\infty} (2n+1) P_n(\mu) \sum_{l=n+4,2}^{\infty} i^l \Lambda_l \quad (\text{B33})$$

B.3.3. A_ξ

Using Eq. (B6) we represent the coefficient A_ξ as $A_\xi = (\Delta - 3D_r - D_{\mu\mu} - 2r\mu D_r D_\mu) \Phi$, thus reducing it to the combination of Eqs. (B28-B31). Let us collect separately the terms in the single sum and the terms in the double sum

$$A_\xi = 4\pi \sum_{n=0}^{\infty} i^n P_n(\mu) \left[-\tilde{\Upsilon}_n + (3+2n)\tilde{\Gamma}_n \right] + 4\pi \sum_{n=0}^{\infty} (2n+1) P_n(\mu) \sum_{l=n+2,2}^{\infty} i^l \left[2\tilde{\Gamma}_l + \frac{1}{2} ((l-1)(l-2) - n(n+1)) \Lambda_l \right] \quad (\text{B34})$$

We again separate the first term in the double sum, noting that there is an additional cancellation of Λ_{n+2} contribution

$$A_\xi = 4\pi \sum_{n=0}^{\infty} i^n P_n(\mu) \left[-\tilde{\Upsilon}_n + (2n+3)\tilde{\Gamma}_n - 2(2n+1)\tilde{\Gamma}_{n+2} \right] + 4\pi \sum_{n=0}^{\infty} (2n+1) P_n(\mu) \sum_{l=n+4,2}^{\infty} i^l \left[2\tilde{\Gamma}_l + \frac{1}{2} ((l-1)(l-2) - n(n+1)) \Lambda_l \right] \quad (\text{B35})$$

and then shift $l \rightarrow l+2$ in the Λ part of the double sum to select Λ_{n+4} which has the same scaling at $kr \rightarrow 0$ as the terms in the single sum

$$A_\xi = 4\pi \sum_{n=0}^{\infty} i^n P_n(\mu) \left[-\tilde{\Upsilon}_n + (2n+3)\tilde{\Gamma}_n - 2(2n+1)\tilde{\Gamma}_{n+2} + (2n+1)(2n+3)\Lambda_{n+4} \right] + 4\pi \sum_{n=0}^{\infty} (2n+1) P_n(\mu) \sum_{l=n+4,2}^{\infty} i^l \left[2\tilde{\Gamma}_l + \frac{1}{2} ((l+1)l - n(n+1)) \Lambda_{l+2} \right] \quad (\text{B36})$$

which gives our original expression.

B.3.4. D_ξ

The last coefficient, D_ξ is different from the ones that have just been considered in that its multipoles are linked to multipoles of the power spectrum of the opposite parity. While even multipoles of E_n , the only expected to be present, give rise to even multipoles of A_ξ, B_ξ and C_ξ , they create odd multipoles of the D_ξ . As a consequence, D_ξ cannot be assembled using just even operators that we have studied. The additional odd derivative that we need is just

$$\frac{\partial}{\partial \mu} P_l(\mu) = \sum_{n=(1,0),2}^{l-1} P_n(\mu) \quad (\text{B37})$$

(here summation starts with unity if l is even, and zero if l is odd, $l=0$ term is absent) which allows us to write

$$\begin{aligned} rD_\mu D_r (j_l(kr) P_l(\mu)) &= \frac{\partial}{\partial \mu} [D_r j_l(kr) P_l(\mu)] = -\tilde{\Gamma}_l(r) \frac{\partial}{\partial \mu} P_l(\mu) - \Lambda_l(r) \sum_{n=(0,1),2}^{l-2} (2n+1) \frac{\partial}{\partial \mu} P_n(\mu) \\ &\rightarrow -\tilde{\Gamma}_l(r) \sum_{n=(1,0),2}^{l-1} (2n+1) P_n(\mu) - \frac{1}{2} \Lambda_l(r) \sum_{n=(1,0),2}^{l-1} (l+n)(l-n-1)(2n+1) P_n(\mu) \end{aligned} \quad (\text{B38})$$

Reverting the summation order again in the full multipole expansion, $\sum_{l=0}^{\infty} \sum_{n=(1,0),2}^{l-1} = \sum_{n=0}^{\infty} \sum_{l=n+1,2}^{\infty}$, and shifting the summation index in Λ_l part by two, $l \rightarrow l+2$, we obtain the Eq. (B15).

C. CORRELATION OF THE SYNCHROTRON INTENSITY IN AXISYMMETRIC MAGNETIC FIELD FOR $\gamma = 2$

For $\gamma = 2$ we have the following relations

$$\langle H_{\perp}^2 \rangle = \langle H_x^2 + H_y^2 \rangle = \sigma_{xx} + \sigma_{yy} \quad (C1)$$

$$\langle H_{\perp}^4 \rangle = \langle (H_x^2 + H_y^2)^2 \rangle = 3\sigma_{xx}^2 + 3\sigma_{yy}^2 + 2\sigma_{xx}\sigma_{yy} + 4\sigma_{xy}^2 \quad (C2)$$

$$\langle H_{\perp}^2(\mathbf{x}_1) H_{\perp}^2(\mathbf{x}_2) \rangle = \langle (H_x^2 + H_y^2)_1 (H_x^2 + H_y^2)_2 \rangle = \quad (C3)$$

$$= \langle H_x^2(\mathbf{x}_1) H_x^2(\mathbf{x}_2) \rangle + \langle H_x^2(\mathbf{x}_1) H_y^2(\mathbf{x}_2) \rangle + \langle H_y^2(\mathbf{x}_1) H_x^2(\mathbf{x}_2) \rangle + \langle H_y^2(\mathbf{x}_1) H_y^2(\mathbf{x}_2) \rangle$$

$$= \sigma_{xx}^2 + 2\sigma_{xx}\sigma_{yy} + \sigma_{yy}^2$$

$$+ 2\langle H_x(\mathbf{x}_1) H_x(\mathbf{x}_2) \rangle^2 + 2\langle H_x(\mathbf{x}_1) H_y(\mathbf{x}_2) \rangle^2 + 2\langle H_y(\mathbf{x}_1) H_x(\mathbf{x}_2) \rangle^2 + 2\langle H_y(\mathbf{x}_1) H_y(\mathbf{x}_2) \rangle^2$$

$$\langle [H_{\perp}^2(\mathbf{x}_1) - H_{\perp}^2(\mathbf{x}_2)]^2 \rangle = 2\langle H_{\perp}^4 \rangle - 2\langle H_{\perp}^2(\mathbf{x}_1) H_{\perp}^2(\mathbf{x}_2) \rangle =$$

$$= 4\sigma_{xx}^2 + 4\sigma_{yy}^2 + 8\sigma_{xy}^2$$

$$- 4\langle H_x(\mathbf{x}_1) H_x(\mathbf{x}_2) \rangle^2 - 4\langle H_x(\mathbf{x}_1) H_y(\mathbf{x}_2) \rangle^2 - 4\langle H_y(\mathbf{x}_1) H_x(\mathbf{x}_2) \rangle^2 - 4\langle H_y(\mathbf{x}_1) H_y(\mathbf{x}_2) \rangle^2$$

$$= 4\sigma_x^2 D_{xx} - D_{xx}^2 + 4\sigma_y^2 D_{yy} - D_{yy}^2 + 8\sigma_{xy} D_{xy} - 2D_{xy}^2 \quad (C4)$$

where we have used the fact that the correlation tensor is symmetric and have denoted the same point 2D covariance matrix by $\sigma_{ij} \equiv \langle H_i H_j \rangle$. The final expression can be written in the manifestly 2D-invariant tensor form

$$\langle H_{\perp}^4 \rangle - \langle H_{\perp}^2 \rangle^2 = 2 \sum_{i,j=1}^2 \sigma_{ij} \sigma_{ji} \quad (C5)$$

$$\langle H_{\perp}^2(\mathbf{x}_1) H_{\perp}^2(\mathbf{x}_2) \rangle - \langle H_{\perp}^2 \rangle^2 = 2 \sum_{i,j=1}^2 \xi_{ij} \xi_{ji} \quad (C6)$$

$$\langle [H_{\perp}^2(\mathbf{x}_1) - H_{\perp}^2(\mathbf{x}_2)]^2 \rangle = \sum_{i,j=1}^2 (4\sigma_{ij} D_{ji} - D_{ij} D_{ji}) \quad (C7)$$

The correlation function of the synchrotron intensity signal $I(\mathbf{X}) \propto \int dz H_{\perp}^2(\mathbf{X}, z)$ is then given by

$$\begin{aligned} \langle I(\mathbf{X}_1) I(\mathbf{X}_2) \rangle - \langle I(\mathbf{X}_1) \rangle^2 &\propto \int dz_1 \int dz_2 [\langle H_{\perp}^2(\mathbf{X}_1, z_1) H_{\perp}^2(\mathbf{X}_2, z_2) \rangle - \langle H_{\perp}^2(\mathbf{X}_1, z_1) \rangle \langle H_{\perp}^2(\mathbf{X}_2, z_2) \rangle] = \\ &= 2 \int dz_+ \int dz \xi_{ij}(\mathbf{X}, z) \xi_{ij}(\mathbf{X}, z) . \end{aligned} \quad (C8)$$

Correspondingly, the structure function is

$$\begin{aligned} \langle [I(\mathbf{X}_1) - I(\mathbf{X}_2)]^2 \rangle &\propto \left\langle \left[\int dz_1 H_{\perp}^2(\mathbf{X}_1, z_1) - \int dz_2 H_{\perp}^2(\mathbf{X}_2, z_2) \right]^2 \right\rangle = \\ &= \int dz_+ \int dz \{ 4\sigma_{ij} [D_{ji}(\mathbf{X}, z) - D_{ji}(0, z)] - [D_{ij}(X, z) D_{ij}(X, z) - D_{ji}(0, z) D_{ij}(0, z)] \} . \end{aligned} \quad (C9)$$

D. GEOMETRICAL FUNCTIONS

The synchrotron correlation function in approximation of the current paper is expressed via the trace of the 2D projection of the spectral tensor that describes the given type of waves. We have encountered the multipole expansions of the following angular functions that represent the 2D angular dependence of the traces of the Fast, Alfvén and Slow projected spectra

$$G_p^F(\theta) = \frac{1}{2\pi} \int_0^{2\pi} d\psi e^{-ip\psi} \frac{\sin^2 \psi}{1 - \cos^2 \psi \sin^2 \theta} , \quad (D1)$$

$$G_p^A(\theta) = \frac{1}{2\pi} \int_0^{2\pi} d\psi e^{-ip\psi} \frac{\cos^2 \theta}{1 - \cos^2 \psi \sin^2 \theta} . \quad (D2)$$

The two angular functions are related by $G_p^A(\theta) + \sin^2 \theta G_p^F(\theta) = \delta_{p0}$. In Figure D1 we plot the behaviour of the multipoles up to $p = 6$ as the functions of the symmetry axis orientation angle θ .

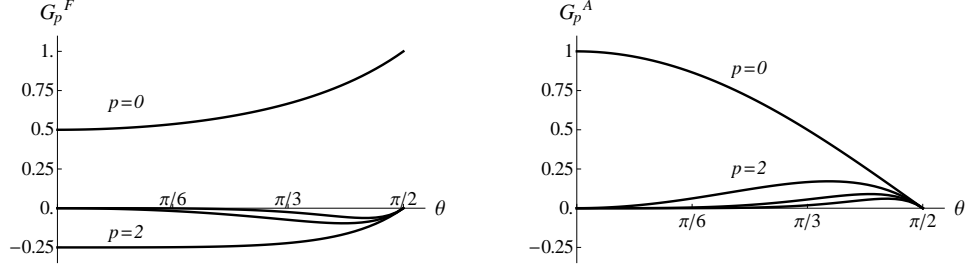


FIG. D1.— Low multipole behaviour for multipole decomposition of the traces of the spectral tensors for the Fast and Slow (left, general F -type tensor) and Alfvén (right) waves.

E. CORRELATIONS OF THE POLARIZATION COMPONENTS OF THE SYNCHROTRON RADIATION

E.1. Correlation of Stokes parameters

Synchrotron intensity is just one of the characteristics of synchrotron emission. Studies of the statistics of synchrotron polarization can be very promising (see Waelkens et al 2009). Below we discuss how the approach in the main part of the paper be generalized to study other Stocks parameters and their combinations. In what follows we use the realistic model of MHD turbulence that we advocate in the paper. For the sake of simplicity we assume that $\gamma = 2$. A study of γ dependence will be done in the subsequent papers.

Complete description of the radiation incoming from the direction \mathbf{X} on the sky is encoded in the polarization matrix

$$\mathbf{P}(\mathbf{X}) = \begin{pmatrix} I + Q & U + iV \\ U - iV & I - Q \end{pmatrix} = I(\mathbf{X}) \begin{pmatrix} 1 & 0 \\ 0 & 1 \end{pmatrix} + \begin{pmatrix} Q(\mathbf{X}) & U(\mathbf{X}) + iV(\mathbf{X}) \\ U(\mathbf{X}) - iV(\mathbf{X}) & -Q(\mathbf{X}) \end{pmatrix} \quad (\text{E1})$$

where Q, U, V are well-known Stokes parameters.

Here we shall limit our consideration to the linear polarization, described by Q and U . We are interested in the correlation between two matrixes $\langle \mathbf{P}(\mathbf{X})\mathbf{P}(\mathbf{X}') \rangle$. Such correlation is convenient to separate into parts based on transformation rules under rotation of the coordinate frame. This gives rise to the

$$\text{scalar : } \langle I(\mathbf{X})I(\mathbf{X}') \rangle \quad \text{"vector" : } \begin{pmatrix} \langle I(\mathbf{X})Q(\mathbf{X}') \rangle \\ \langle I(\mathbf{X})U(\mathbf{X}') \rangle \end{pmatrix} \quad \text{"tensor" : } \begin{pmatrix} \langle Q(\mathbf{X})Q(\mathbf{X}') \rangle & \langle Q(\mathbf{X})U(\mathbf{X}') \rangle \\ \langle U(\mathbf{X})Q(\mathbf{X}') \rangle & \langle U(\mathbf{X})U(\mathbf{X}') \rangle \end{pmatrix} \quad (\text{E2})$$

parts. Here we put "vector" and "tensor" in the quotation marks, since they rotate with twice the angle Φ of the rotation of the coordinate system

$$\begin{pmatrix} Q' \\ U' \end{pmatrix} = \begin{pmatrix} \cos 2\Phi & \sin 2\Phi \\ -\sin 2\Phi & \cos 2\Phi \end{pmatrix} \begin{pmatrix} Q \\ U \end{pmatrix} \quad (\text{E3})$$

The "vector" terms describe cross-correlation between the intensity and linear polarization, while the "tensor" part describes correlation between polarizations themselves.

For synchrotron radiation in $\gamma = 2$ case, following Waelkens et al. (2009),

$$I(\mathbf{X}) \propto n_e \int dz (H_{xx}^2 + H_{yy}^2) \quad (\text{E4})$$

$$Q(\mathbf{X}) \propto p n_e \int dz (H_{xx}^2 - H_{yy}^2) \quad (\text{E5})$$

$$U(\mathbf{X}) \propto p n_e \int dz 2H_{xx}H_{yy} \quad (\text{E6})$$

where $p = \sqrt{Q^2 + U^2}/I$ is the degree of linear polarization and n_e is the density of the electrons, both assumed constant over the line-of-sight range where the signal forms. These expressions are in the laboratory frame x, y in which Q and U parameters are defined.

Evaluation of the structure functions that involve polarization are similar to the computations that led to Eq. (48) for intensity. Using for brevity notation $D_{IU}(\mathbf{R}) = \langle [I(\mathbf{X}_1) - I(\mathbf{X}_2)] [U(\mathbf{X}_1) - U(\mathbf{X}_2)] \rangle$ and so on, the expressions for individual correlation components are

$$D_{IQ} \propto 4p \int dz \times \quad (\text{E7})$$

$$\left[\sigma_{xx} D_{xx}(\mathbf{R}, z) - \sigma_{yy} D_{yy}(\mathbf{R}, z) - \frac{1}{4} (D_{xx}(\mathbf{R}, z)^2 + D_{yy}(\mathbf{R}, z)^2) \right] - \left[\mathbf{R} \rightarrow 0 \right]$$

$$D_{IU} \propto 4p \int dz \times \quad (\text{E8})$$

$$\left[\sigma_{xy} (D_{xx}(\mathbf{R}, z) + D_{yy}(\mathbf{R}, z)) + (\sigma_{xx} + \sigma_{yy}) D_{xy}(\mathbf{R}, z) - \frac{1}{2} D_{xy}(\mathbf{R}, z) (D_{xx}(\mathbf{R}, z) + D_{yy}(\mathbf{R}, z)) \right] - \left[\mathbf{R} \rightarrow 0 \right]$$

$$D_{QQ} \propto 4p^2 \int dz \times \left[\sigma_{xx} D_{xx}(\mathbf{R}, z) + \sigma_{yy} D_{yy}(\mathbf{R}, z) - 2\sigma_{xy} D_{xy}(\mathbf{R}, z) - \frac{1}{4} (D_{xx}(\mathbf{R}, z)^2 + D_{yy}(\mathbf{R}, z)^2 - 2D_{xy}(\mathbf{R}, z)^2) \right] - [\mathbf{R} \rightarrow 0] \quad (\text{E9})$$

$$D_{UU} \propto 4p^2 \int dz \times \left[\sigma_{yy} D_{xx}(\mathbf{R}, z) + \sigma_{xx} D_{yy}(\mathbf{R}, z) + 2\sigma_{xy} D_{xy}(\mathbf{R}, z) - \frac{1}{2} (D_{xx}(\mathbf{R}, z) D_{yy}(\mathbf{R}, z) + D_{xy}(\mathbf{R}, z)^2) \right] - [\mathbf{R} \rightarrow 0] \quad (\text{E10})$$

$$D_{QU} \propto 4p^2 \int dz \times \left[\sigma_{xy} (D_{xx}(\mathbf{R}, z) - D_{yy}(\mathbf{R}, z)) + (\sigma_{xx} - \sigma_{yy}) D_{xy}(\mathbf{R}, z) - \frac{1}{2} D_{xy}(\mathbf{R}, z) (D_{xx}(\mathbf{R}, z) - D_{yy}(\mathbf{R}, z)) \right] - [\mathbf{R} \rightarrow 0] \quad (\text{E11})$$

where $[\mathbf{R} \rightarrow 0]$ signifies the same integrand as in the main expression but evaluated at zero separation \mathbf{R} between the line of sights. We remark that U or Q correlations with intensity I are proportional to the first power of the degree of polarization, while polarization cross-correlations are quadratic. For weakly polarized signal it may be easier to measure the former.

The trace of the polarization correlation "tensor" provides the frame invariant measure

$$D_{QQ} + D_{UU} \propto 4p^2 \int dz \left[(\sigma_{xx} + \sigma_{yy}) (D_{xx}(\mathbf{R}, z) + D_{yy}(\mathbf{R}, z)) - \frac{1}{4} (D_{xx}(\mathbf{R}, z) + D_{yy}(\mathbf{R}, z))^2 \right] - [\mathbf{R} \rightarrow 0] \quad (\text{E12})$$

In Eqs (E7-E11) the 2D components of the magnetic field correlation (structure) tensor D_{ij} refer to the laboratory frame, in which the Stokes Q and U are measured. Let us rewrite the same expressions using D_{ij} in the frame aligned with the symmetry axis $\hat{\Lambda}$, where theoretical calculations for axisymmetric turbulence are more straightforward. From here onwards, $D^+ = D_{xx} + D_{yy}$, $D^- = D_{xx} - D_{yy}$ and $D^\times = D_{xy}$ refer to components in such a symmetry frame, while Φ is the angle between $\hat{\Lambda}$ and the laboratory x -axis. Limiting ourselves to the linearized approximation, applicable, as in Eq. (48), at small scales, we find

$$D_{IQ} \propto 2p (\sigma_{xx} + \sigma_{yy}) \int dz \left[(D^-(\mathbf{R}, z) + \epsilon D^+(\mathbf{R}, z)) \cos 2\Phi - 2D^\times(\mathbf{R}, z) \sin 2\Phi \right] - [\mathbf{R} \rightarrow 0] \quad (\text{E13})$$

$$D_{IU} \propto 2p (\sigma_{xx} + \sigma_{yy}) \int dz \left[(D^-(\mathbf{R}, z) + \epsilon D^+(\mathbf{R}, z)) \sin 2\Phi + 2D^\times(\mathbf{R}, z) \cos 2\Phi \right] - [\mathbf{R} \rightarrow 0] \quad (\text{E14})$$

$$D_{QQ} \propto 2p^2 (\sigma_{xx} + \sigma_{yy}) \int dz \left[D^+(\mathbf{R}, z) + \epsilon D^-(\mathbf{R}, z) \cos 4\Phi - 2\epsilon D^\times(\mathbf{R}, z) \sin 4\Phi \right] - [\mathbf{R} \rightarrow 0] \quad (\text{E15})$$

$$D_{UU} \propto 2p^2 (\sigma_{xx} + \sigma_{yy}) \int dz \left[D^+(\mathbf{R}, z) - \epsilon D^-(\mathbf{R}, z) \cos 4\Phi + 2\epsilon D^\times(\mathbf{R}, z) \sin 4\Phi \right] - [\mathbf{R} \rightarrow 0] \quad (\text{E16})$$

$$D_{QU} \propto 2p^2 \epsilon (\sigma_{xx} + \sigma_{yy}) \int dz \left[D^-(\mathbf{R}, z) \sin 4\Phi + 2D^\times(\mathbf{R}, z) \cos 4\Phi \right] - [\mathbf{R} \rightarrow 0] \quad (\text{E17})$$

The frame invariant combinations are

$$D_{QQ} + D_{UU} \propto 4p^2 (\sigma_{xx} + \sigma_{yy}) \int dz D^+(\mathbf{R}, z) - [\mathbf{R} \rightarrow 0], \quad (\text{E18})$$

and, for completeness, the intensity structure function from Eq (48)

$$D_{II} \propto 2 (\sigma_{xx} + \sigma_{yy}) \int dz \left[(D^+(\mathbf{R}, z) + \epsilon D^-(\mathbf{R}, z)) \right] - [\mathbf{R} \rightarrow 0] \quad (\text{E19})$$

The magnetic field variance anisotropy parameter, ϵ , is defined in Eq. (50).

E.2. Angular properties of the polarization correlations

Let us turn to the angular dependence of the polarization functions. Our study of the intensity of the synchrotron in the main text can be reformulated as the following rules of correspondence between the different parts of the magnetic correlation tensor and the multipoles of the synchrotron correlations they contribute to

$$\int dz D^+(\mathbf{R}, z) \rightarrow \tilde{D}_n \propto \sum_{s=-\infty}^{\infty} E_s G_{n-s}(\theta) \quad (\text{E20})$$

$$\int dz D^-(\mathbf{R}, z) \rightarrow \tilde{D}_n \propto \sum_{s=-\infty}^{\infty} -\frac{1}{2} (E_{s+2} + E_{s-2}) G_{n-s}(\theta) \quad (\text{E21})$$

where E_s are coefficients of multipole expansion of the projected power spectrum $E(K, \psi)$ wrt the sky orientation angle of the wave vector ψ and $G_p(\theta)$ are multipoles of one of the geometric functions $G(\theta, \psi)$ (see Appendix D) that describes the specific turbulent mode. This rule reproduces Eqs. (61) and (65) when applied, correspondingly, to E and F -type modes of the general axisymmetric tensor Eq. (51).

To study polarization one also needs the additional component

$$\int dz D^\times(\mathbf{R}, z) \rightarrow \tilde{D}_n \propto \sum_{s=-\infty}^{\infty} \frac{i}{4} (E_{s+2} - E_{s-2}) G_{n-s}(\theta). \quad (\text{E22})$$

While D^+ and D^- combinations give rise to real \tilde{D}_n coefficients and, thus, symmetric $\sim \cos n\phi$ dependence of the synchrotron correlations, D^\times contributes the imaginary part to \tilde{D}_n and antisymmetric $\sim \sin n\phi$ signal correlation behaviour. Antisymmetric contribution is not present if the mode tensor is isotropic, when $G_{n-p} = \delta_{np}$. Presence of the antisymmetric, $\sin n\phi$, behaviour in the correlation patterns of polarization is a direct indication of the F -term contribution to the spectral tensor structure. It is expected at some level for Alfvén and Fast modes.

The resulting multipole decomposition of the polarization structure functions is

$$(\tilde{D}_{IQ})_n \propto 2p AC_n(m) R^{1+m} \sum_{s=-\infty}^{\infty} \left[\left(-\frac{1}{2} (E_{s+2} + E_{s-2}) + \epsilon E_s \right) \cos 2\Phi + \frac{i}{2} (E_{s+2} - E_{s-2}) \sin 2\Phi \right] G_{n-s}^{(A,F,S)} \quad (\text{E23})$$

$$(\tilde{D}_{IU})_n \propto 2p AC_n(m) R^{1+m} \sum_{s=-\infty}^{\infty} \left[\left(-\frac{1}{2} (E_{s+2} + E_{s-2}) + \epsilon E_s \right) \sin 2\Phi - \frac{i}{2} (E_{s+2} - E_{s-2}) \cos 2\Phi \right] G_{n-s}^{(A,F,S)} \quad (\text{E24})$$

$$(\tilde{D}_{QQ})_n \propto 2p^2 AC_n(m) R^{1+m} \sum_{s=-\infty}^{\infty} \left[E_s - \frac{\epsilon}{2} (E_{s+2} + E_{s-2}) \cos 4\Phi + \frac{i\epsilon}{2} (E_{s+2} - E_{s-2}) \sin 4\Phi \right] G_{n-s}^{(A,F,S)} \quad (\text{E25})$$

$$(\tilde{D}_{UU})_n \propto 2p^2 AC_n(m) R^{1+m} \sum_{s=-\infty}^{\infty} \left[E_s + \frac{\epsilon}{2} (E_{s+2} + E_{s-2}) \cos 4\Phi - \frac{i\epsilon}{2} (E_{s+2} - E_{s-2}) \sin 4\Phi \right] G_{n-s}^{(A,F,S)} \quad (\text{E26})$$

$$(\tilde{D}_{QU})_n \propto 2p^2 AC_n(m) R^{1+m} \sum_{s=-\infty}^{\infty} \left[-\frac{1}{2} (E_{s+2} + E_{s-2}) \sin 4\Phi - \frac{i}{2} (E_{s+2} - E_{s-2}) \cos 4\Phi \right] G_{n-s}^{(A,F,S)} \quad (\text{E27})$$

where $G_{n-s}^{(A,F,S)}(\theta)$ stands for one of the particular geometrical mode functions, Alfvén, Fast or Slow, or their combinations. It depends, parametrically on the angle θ between the mean magnetic field direction and the line of sight.

Polarization provides new avenues to link properties of the magnetized turbulence to observables. The most direct measure of the turbulence spectral anisotropy is provided by the trace of the synchrotron polarization matrix

$$\left(\tilde{D}_{QQ+UU} \right)_n \propto 4p^2 A_{(A,F,S)} C_n(m) R^{1+m} \sum_{s=-\infty}^{\infty} E_s G_{n-s}^{(A,F,S)}(\theta) \quad (\text{E28})$$

It may be possible to determine the direction of the axis of symmetry (mean magnetic field) by measuring separately symmetric (cos) and antisymmetric (sin) patterns of the correlations. For example $\tan 2\Phi = \text{Re}(D_{IU})_n / \text{Re}(D_{IQ})_n$ can be compared with the direction obtained from elongation of iso-correlation contours of intensity. And when symmetry direction is determined, ϵ parameter can be estimated from $\text{Im}(D_{QU})_n / \text{Im}(D_{IU})_n = p\epsilon$ evaluated in the symmetry frame $\Phi = 0$, if there is a non-vanishing imaginary contribution to correlation multipoles from D_{xy} .

We may conclude that angular and scaling dependencies of the correlations of synchrotron polarization and intensity, Eqs (E13-E19), contain wealth of information about orientation of the symmetry axis, ϵ parameter and full projected correlation tensor of the magnetic field. Redundancies build into different signals allow for multiple cross-checks. Detail study of the possibilities that synchrotron polarization opens for studies of anisotropic magnetized turbulence is a subject of the future work.

E.3. Correlations of the line-of-sight component of the magnetic field

Faraday rotation measures provide a valuable source information about magnetic turbulence. However, the models of turbulence adopted in earlier studies were models of isotropic turbulence. Below we calculate the statistics of Faraday rotation measures which is based on a realistic MHD turbulence model. The measures we deal with do not depend on the cosmic ray spectral index.

Study of intensity and linear polarization of the synchrotron led us to the discussion of the orthogonal to the line-of-sight components of the magnetic field. Let us in conclusion collect the results for the projected correlation of the line-of-sight component $D_{zz}(\mathbf{R}) = \int dz \langle H_z(\mathbf{x}_1) H_z(\mathbf{x}_2) \rangle$. This quantity describes the correlation of Faraday phase $\langle \phi(\mathbf{X}_1) \phi(\mathbf{X}_2) \rangle$ and is important in polarization studies. We present the results for the line-of-sight component here to complete our statistical formalism.

From Eq. (51) one immediately obtains the sky-projected structure function between the line-of-sight (z) components of the magnetic field as

$$D_{zz}(\mathbf{R}) = \int dz \langle H_z H_z \rangle \propto \frac{1}{(2\pi)^2} \int d^2 K e^{i\mathbf{K} \cdot \mathbf{R}} \left[E(\mathbf{K}) + F(\mathbf{K}) \frac{\cos^2 \theta}{1 - \cos^2 \psi \sin^2 \theta} \right] \quad (\text{E29})$$

Spectral representation of different turbulence modes can be expressed again using combinations of the geometrical functions introduced in Appendix D. Namely, using Eqs. (69, 77, 79, 73)

$$\begin{array}{lll}
 \text{Alfven} & F(\mathbf{K}) = -E(\mathbf{K}) & D_{zz} \propto E(\mathbf{K}) \sin^2 \theta G^F \\
 \text{Slow (high } \beta) & E(\mathbf{K}) = 0, & D_{zz} \propto F(\mathbf{K}) G^A \\
 \text{Alfven + Slow (strong)} & F(\mathbf{K}) = 0 & D_{zz} \propto E(\mathbf{K}) \\
 \text{Fast (low } \beta) & E(\mathbf{K}) = 0, F(\mathbf{K}) = F(K) & D_{zz} \propto F(K) G^A \\
 \text{Fast (high } \beta) & E(\mathbf{K}) = 0, F(\mathbf{K}) = F(K) (1 - \cos^2 \psi \sin^2 \theta) & D_{zz} \propto F(K) \cos^2 \theta
 \end{array} \quad (\text{E30})$$

Multiple decomposition of the angular dependence of the $D_{zz}(\mathbf{R})$ is described by convolution of the multiple decompositions of the spectral and geometrical functions in Eq. (E30). Variation of the direction of the mean magnetic field along the line of sight leads to isotropization of the D_{zz} , in a similar way that we have studied for the synchrotron intensity.

REFERENCES

- Abramovitz M. & Stegun I. 1965, Handbook of Mathematical Functions, Dover, NY
- Armstrong, J. W., Rickett, B. J., & Spangler, S. R. 1995, ApJ, 443, 209
- Batchelor, G. K. 1946, Royal Society of London Proceedings Series A, 186, 480
- Beresnyak, A., Jones, T. W., & Lazarian, A. 2009, ApJ, 707, 1541
- Beresnyak, A., & Lazarian, A. 2010, ApJ, 722, L110
- Beresnyak, A., & Lazarian, A. 2006, ApJ, 640, L175
- Beresnyak, A., & Lazarian, A. 2009, ApJ, 702, 1190
- Boldyrev, S. 2006, Physical Review Letters, 96, 115002
- Boldyrev, S. 2005, ApJ, 626, L37
- Brunetti G. & Lazarian A., 2007 MNRAS, 378, 245
- Burkhart, B., Falceta-Gonçalves, D., Kowal, G., & Lazarian, A. 2009, ApJ, 693, 250
- Burkhart, B., Stanimirović, S., Lazarian, A., & Kowal, G. 2010, ApJ, 708, 1204
- Burlaga, L. F., & Viñas, A. F. 2004, Geophys. Res. Lett., 31, 16807
- Burlaga, L. F., & F-Viñas, A. 2004, Journal of Geophysical Research (Space Physics), 109, 12107
- Burlaga, L. F., & -Viñas, A. F. 2005, Physica A Statistical Mechanics and its Applications, 356, 375
- Burlaga, L. F., & F-Viñas, A. 2006, Physica A Statistical Mechanics and its Applications, 361, 173
- Burlaga, L. F., Ness, N. F., & Acuña, M. H. 2006, ApJ, 642, 584
- Burlaga, L. F., Viñas, A. F., Ness, N. F., & Acuña, M. H. 2006, ApJ, 644, L83
- Burlaga, L. F., Ness, N. F., & Acuña, M. H. 2009, ApJ, 691, L82
- Burlaga, L. F., Ness, N. F., & Acuña, M. H. 2007, ApJ, 668, 1246
- Chandrasekhar, S. 1950, Royal Society of London Philosophical Transactions Series A, 242, 557
- Chepurnov, A. V. 1998, Astronomical and Astrophysical Transactions, 17, 281
- Chepurnov, A., Gordon, J., Lazarian, A., & Stanimirovic, S. 2008, ApJ, 688, 1021
- Chepurnov, A., & Lazarian, A. 2009, ApJ, 693, 1074
- Chepurnov, A., & Lazarian, A. 2010, ApJ, 710, 853
- Chepurnov, A., Lazarian, A., Stanimirović, S., Heiles, C., & Peek, J. E. G. 2010, ApJ, 714, 1398
- Chibisov, G. & Ptuskin, V., 1981, Abstracts of XVII Cosmic Ray Conference
- Cho, J., & Vishniac, E. T. 2000, ApJ, 539, 273
- Cho, J., Lazarian, A., & Vishniac, E. T. 2002, ApJ, 564, 291
- Cho, J., & Lazarian, A. 2002, Physical Review Letters, 88, 245001
- Cho, J., & Lazarian, A. 2003, MNRAS, 345, 325
- Cho, J., & Lazarian, A. 2005, Theoretical and Computational Fluid Dynamics, 19, 127
- Cho, J., & Lazarian, A. 2010, ApJ, 720, 1181
- de Gouveia dal Pino, E. M., & Lazarian, A. 2005, A&A, 441, 845
- Elmegreen, B. G., & Scalo, J. 2004, ARA&A, 42, 211
- Esquivel, A., & Lazarian, A. 2005, ApJ, 631, 320
- Esquivel, A., & Lazarian, A. 2010, ApJ, 710, 125
- Esquivel, A., & Lazarian, A. 2011, ApJ, in press
- Esquivel, A., Lazarian, A., Horibe S., Cho J., Ossenkopf V. and Stutzki J. 2007, MNRAS, 381, 1733
- Enßlin, T. A., Clarke, T., Vogt, C., Waelkens, A., & Schekochihin, A. A. 2010, Highlights of Astronomy, 15, 456
- Enßlin, T. A., Clarke, T., Vogt, C., Waelkens, A., & Schekochihin, A. A. 2009, Revista Mexicana de Astronomia y Astrofisica Conference Series, 36, 209
- Enßlin, T. A., & Vogt, C. 2006, A&A, 453, 447
- Falgarone, E., Lis, D. C., Phillips, T. G., Pouquet, A., Porter, D. H., & Woodward, P. R. 1994, ApJ, 436, 728
- Federrath, C., Roman-Duval, J., Klessen, R. S., Schmidt, W., & Mac Low, M.-M. 2010, A&A, 512, A81
- Federrath, C., Klessen, R. S., & Schmidt, W. 2009, ApJ, 692, 364
- Federrath, C., Klessen, R. S., & Schmidt, W. 2008, ApJ, 688, L79
- Fleishman, G. 2008, Stochastic Theory of Emission, R&C Dynamics, Moscow
- Haverkorn, M. 2010, Astronomical Society of the Pacific Conference Series, 438, 249
- Heyer, M., Gong, H., Ostriker, E., & Brunt, C. 2008, ApJ, 680, 420
- Gaensler et al. 2011, Nature, in press
- Getmantsev G.G. 1959, Sov. Astron. Journ., 36, 422
- Ginzburg, V. 1981, Theoretical physics and Astrophysics, Nauka, Moscow
- Goldreich, P., & Sridhar, S. 1995, ApJ, 438, 763
- Higdon, J. C. 1984, ApJ, 285, 109
- Junklewitz, H., & Enßlin, T. A. 2011, A&A, 530, A88
- Kowal, G., & Lazarian, A. 2010, ApJ, 720, 742
- Kowal, G., Lazarian, A., Vishniac, E. T., & Otmianowska-Mazur, K. 2009, ApJ, 700, 63
- Larson, R. B. 1981, MNRAS, 194, 809
- Lazarian, A. 2009, Space Sci. Rev., 143, 357
- Lazarian, A. 2007, J. Quant. Spec. Radiat. Transf., 106, 225
- Lazarian, A. 2006, ApJ, 645, L25
- Lazarian, A. & Chibisov, G. 1991, Sov. Astron. Lett., 17(3), 208
- Lazarian, A. & Shutenkov, V. 1990, Sov Astron. Lett., 16(4), 297
- Lazarian, A., & Esquivel, A. 2003, ApJ, 592, L37
- Lazarian, A., & Pogosyan, D. 2008, ApJ, 686, 350
- Lazarian, A., & Pogosyan, D. 2006, ApJ, 652, 1348
- Lazarian, A., & Pogosyan, D. 2004, ApJ, 616, 943
- Lazarian, A., & Pogosyan, D. 2000, ApJ, 537, 720
- Lazarian A., Pogosyan D., Esquivel A., 2002, in: Seeing Through the Dust: The Detection of HI and the Exploration of the ISM in Galaxies. Astronomical Society of the Pacific Conference Series, 276, 182
- Lazarian, A., & Vishniac, E. T. 1999, ApJ, 517, 700
- Lazarian A., Pogosyan D., Vázquez-Semadeni E. & Pichardo B., 2001, ApJ, 555, 130
- Longair, M. 2011, High Energy Astrophysics, 3d Edition, CUP
- Liu, A., Tegmark, M., Bowman, J., Hewitt, J., & Zaldarriaga, M. 2009, MNRAS, 398, 401
- Lithwick, Y., & Goldreich, P. 2001, ApJ, 562, 279
- Loeb, A. & Wyithe, J. S. B. 2008, Phys. Rev. Letters, 100, 1301
- Loeb, A. & Zaldarriaga, M. 2004, Phys. Rev. Letters, 92, 1301
- McKee, C. F., & Ostriker, E. C. 2007, ARA&A, 45, 565
- Malkov, M. A., & Diamond, P. H. 2009, ApJ, 692, 1571
- Maron, J., & Goldreich, P. 2001, ApJ, 554, 1175
- Matthaeus, W. H., & Smith, C. 1981, Phys. Rev. A, 24, 2135
- Matthaeus, W. H., Goldstein M. L., Roberts D. A., 1990, J. Geophys. Res. 95, 20673
- Montgomery, D., & Turner, L. 1981, Physics of Fluids, 24, 825
- Narayan, R., & Medvedev, M. V. 2001, ApJ, 562, L129
- Oughton, S., Rädler, K.-H., & Matthaeus, W. H. 1997, Phys. Rev. E, 56, 2875
- Padoan, P., Jimenez, R., Juvela, M., & Nordlund, A. 2004, ApJ, 604, L49
- Padoan, P., Juvela, M., Kritsuk, A., & Norman, M.-L. 2006, ApJ, 653, L125
- Padoan, P., Juvela, M., Kritsuk, A., & Norman, M. L. 2009, ApJ, 707, L153
- Pen, U.-L., Staveley-Smith, L. and Peterson, J. & Chang, T.-C. 2008, arXiv 0802.3239
- Pohl, M. 1996, A&A, 307, L57
- Rosolowsky, E. W., Pineda, J. E., Kauffmann, J., & Goodman, A. A. 2008, ApJ, 679, 1338
- Rosolowsky, E. W., Goodman, A. A., Wilner, D. J., & Williams, J. P. 1999, ApJ, 524, 887
- Shebalin, J. V., Matthaeus, W. H., & Montgomery, D. 1983, Journal of Plasma Physics, 29, 525
- Schlickeiser, R. 2002, Cosmic ray astrophysics / Reinhard Schlickeiser, Astronomy and Astrophysics Library; Physics and Astronomy Online Library. Berlin: Springer

- Stutzki, J. 1999, Plasma Turbulence and Energetic Particles in Astrophysics, 48
- Tofflemire, B. M., Burkhart, B., & Lazarian, A. 2011, arXiv:1103.3299
- Yan, H., & Lazarian, A. 2008, ApJ, 677, 1401
- Yan, H., & Lazarian, A. 2004, ApJ, 614, 757
- Waelkens, A. H., Schekochihin, A. A., & Enflin, T. A. 2009, MNRAS, 398, 1970
- Westfold, K. C. 1959, ApJ, 130, 241
- Zank, G. P., & Matthaeus, W. H. 1993, Physics of Fluids, 5, 257